Cleaner Chemical Engineering 3 (2022) 100046

Contents lists available at ScienceDirect

Cleaner Chemical Engineering

journal homepage: www.elsevier.com/locate/clce

Bioenergy potential of millet chaff *via* thermogravimetric analysis and combustion process simulation using Aspen Plus

Isah Yakub Mohammed [a,*], Garba Kabir [a], Yousif Abdalla Abakr [b], Michael Atogiba Ayiania Apasiku [c], Feroz Kabir Kazi [d], Lawan Garba Abubakar [e]

[a] Department of Chemical Engineering, Abubakar Tafawa Balewa University, PMB 0248 Bauchi, Nigeria
[b] Department of Mechanical, Materials and Manufacturing Engineering, University of Nottingham Malaysia, Jalan Broga, Semenyih 43500, Selangor Darul Eshan, Malaysia
[c] Department of Biological Systems Engineering, Washington State University, L.J. Smith Hall, 1935 E. Grimes Way, Pullman, WA, 99164-6120, United States
[d] Department of Engineering and Mathematics, Sheffield Hallam University, City Campus, Howard Street, Sheffield, S1 1WB, UK
[e] Department of Agricultural and Bioresource Engineering, Abubakar Tafawa Balewa University, PMB 0248 Bauchi, Nigeria

ARTICLE INFO

Keywords:
Millet chaff
Characterisation
Proxanal
Ultanal
Combustion
Thermogravimetric
Simulation
Aspen Plus

ABSTRACT

Millet chaff constitutes one of the most abundant agro-residues in the sub-Saharan Africa and its utilisation as a feedstock in developing sustainable bioenergy solutions is very sketchy. This study presents the first comprehensive physicochemical and combustion characteristics of millet chaff via thermogravimetric analysis and process simulation using Aspen Plus. The millet chaff sample was collected and assessed as received for proximate and ultimate analyses. The results showed the biomass has 71.25 wt%, 15.35 wt%, 13.40 wt% and 13.15 MJ/kg for volatile matter, fixed-carbon, ash content and higher heating value respectively. The material consists of low nitrogen and sulphur content with potassium, aluminium, magnesium, calcium, iron and sodium as the inorganic components. Kinetic study using distributed activation energy model (DAEM) revealed an average frequency factor and activation energy of $1.41 \times 10^{18} (s^{-1})$ and 149.39 kJ/mol. Ignition and burnout temperature in the range of 232-244°C and 430-489°C were recorded. The average combustion thermodynamic parameters; ΔH, ΔG and ΔS were found to be 144.75 kJ/mol, 167.12 kJ/mol and -40.08 J/mol. The combustion process analysis coupled with steam turbine cycle via process simulation revealed an excellent combustion efficiency at air-fuel ratio of 5.14. (stoichiometric air). The power generation and electric efficiency of 0.7kWh/kg and 21.07% respectively were recorded at 24% excess air with minimal environmental impacts. This suggests that millet chaff is a good biomass feedstock suitable for clean bioenergy production.

1. Introduction

Fossil fuels remain the major source of energy globally despite the environmental challenges such as emission of greenhouse gases (GHG) from its utilisation. This trend will continue for decades to come as there are currently no viable alternatives that are competitive in terms of cost and meeting the requirement of the existing fossil fuel processing facilities. To achieve drastic reduction in energy contribution from fossil fuel, agricultural diversification has been identified as part of the measures in terms of developing opportunities for green energy and sustainable production systems. Pearl millet is one of the most grown cereal crops in Africa. It is a C4 plant with high drought tolerance and can be

Abbreviations: DAEM, Distributed activation energy model; AFR, Air-fuel ratio; GHG, Greenhouse gases; SDG, Sustainable development goal; ICTAC, International Confederation for Thermal Analysis and Calorimetry; C, Carbon; H, Hydrogen; N, Nitrogen; S, Sulphur; O, Oxygen; SO2, Sulphur dioxide; CO2, Carbo dioxide; CO, Carbon monoxide; NO2, Nitogen dioxide; NO, Nitric oxide; N2O, Nitrous oxide; MCHF, Millet chaff; NG, Napier grass; BGS, Bambara ground nut shell; OPF, Oil palm frond; PNS, Peanut shell; AZP, Adzuki been pod; DCMP, Decomposed products; CMBPD, Combustion products; ASFHFG, Ash-free hot flue gas; CFGAS, Cold flue gas; HPSTM, High-pressure steam; LPSTM, low-pressure steam; CWTER, Cold water; FTIR, Fourier transform infrared; TGA, Thermogravimetric analyze; TG, Thermogravimetric; ΔH, Change in enthalpy; ΔS, Change in entropy; ΔG, Change in Gibbs free energy; K_B, Boltzmann constant; h, Planck's constant; DTG, Derivative thermogravimetric; Na, Sodium; Ca, Calcium; K, Potassium; Mg, Magnesium; Al, Aluminium; EDX, Energy dispersive X-ray; ICP-MS, Inductively coupled plasma mass spectrometer; VL, Vertical line; TL, Tangential line; T_{ign}, Ignition temperature; T_{bnt}, Burnout temperature; f(E), Activation energy distribution function; E_A, Activation energy; β, Heating rate; k_0, Pre-exponential factor; NRTL, Non-random two-liquid; CYCL, Cyclone; FGHX, Flue gas heat exchanger; S-TURBIN, Steam turbine; W-COND, Condenser; W-PUMP, Pump; CHP, Combined heat and power; CE, Combustion efficiency; EE, Electric efficiency.

* Corresponding author.
E-mail address: yimohd@atbu.edu.ng (I.Y. Mohammed).

https://doi.org/10.1016/j.clce.2022.100046
Received 25 May 2022; Received in revised form 2 July 2022; Accepted 5 July 2022
2772-7823/© 2022 The Author(s). Published by Elsevier Ltd. This is an open access article under the CC BY-NC-ND license (http://creativecommons.org/licenses/by-nc-nd/4.0/)

cultivated with little to no nutrient input or grown on marginal lands (Nematpour et al., 2020). In 2016, global production of millet was 28.4 million tonnes, led by India with 36% of the world total production. Nigeria is the fifth producer of millet in the world as at 2016 with an annual tonnage of 1.5million tonnes (FAOSTAT of United Nation). Millet chaff is one the agro-residues from millet cultivation. It is the husk after the millet grains are removed from the millet bunch. This material has limited application as a large chunk of it is regarded as waste at dumpsites undergoing open burning. The current Nigerian government policy on Agricultural Promotion (2016-2020) on food sufficiency, which is in consonant with sustainable development goal (SDG2), suggests that a colossal amount of millet chaff will be generated. This will add to the current challenges of solid waste management in the country.

Generally, utilisation of agro-waste for energy generation can be considered sustainable since the materials are regarded as a zero-cost feedstock. In terms of the processes available to obtain energy and energy derivatives, thermochemical conversion technologies such as combustion, pyrolysis and gasification can be adopted to harness the energy potential of the wastes particularly in the rural areas where the agro-waste is available in large quantities. This could be principally advantageous towards attaining the SDG7 in addition to offering environmental and financial benefits to rural communities. Consequently, preliminary evaluation of bioenergy potentials of millet chaff via thermochemical conversion will provide useful details for sustainable design of conversion facilities and suitable conversion pathways. Currently, millet chaff has been grossly underutilised for energy recovery. Only recently, Ryden et al. (2017) reported bioethanol production via biochemical pathway using spent millet chaff from mushroom cultivation. Their findings revealed that the spent millet chaff compost could yield up to 63.9 g of bioethanol/kg dry matter at concentration of 19.6 g/L. The authors further stated that the result obtained from this material is quite lower relative to the bioethanol from sorghum-derived compost with concentration of 45.8 g/L. This observation was attributed to higher cellulose content in the sorghum feedstock. Boubacar Laougé and Merdun (2020) reported thermochemical evaluation of millet chaff under inert and oxidised environments in a thermogravimetric analyser. This technique is quite robust as it allows acquisition of data related to the sample weight loss and decomposition rate with respect to temperature, time, or both under a controlled atmosphere. Data from such assessment provides useful information regarding sample decomposition and mechanisms, which is important for the design of thermochemical conversion systems. The authors established the kinetics and thermodynamics using isoconversional models. Their results indicated that the material has low activation energies under both conditions. However, considerable high heating rates (10, 20, 30, 40, and 50°C/min) were employed in the study which do not allow segregation of individual biomass components decomposition profiles to be established. Vyazovkin et al. (2011) reported that doubling of heating rate typically causes the kinetic curve to shift by approximately 15°C, which in turn affects the activation energy and frequency factor values. Therefore, further investigations of kinetics and thermodynamics of millet chaff at moderate heating rates as recommended by the International Confederation for Thermal Analysis and Calorimetry (ICTAC) need to be carried out.

Biomass fired power plant is considered one of the promising options for power generation with high possibilities of having economic benefit in addition to meeting environmental requirements (Afgan et al., 2007). This technology has a wide application ranging from small-scale boilers to industrial furnaces dedicated to heat and/or power generation. It also fits well in regions without traditional fossil resources for meeting the electricity demand. However, increase in nitrogen oxides (NO_2, NO and N_2O, known as NOx) and carbon monoxide (CO) levels in the flue gas remains a challenge. NOx emission largely depends on burner design and fuel quality. This suggests that individual biomass material needs to be investigated to determine its suitability as a fuel in combustion process since new burner designs suitable for biomass firing are being developed (Bermúdez et al., 2020). Design of combustion equipment normally involves a laborious trial design approach to identify the most suitable configuration, which is very expensive (Bermúdez et al., 2020; Smith et al., 2020). Application of process modelling, and simulation plays a very important role in process development. It allows evaluation of process performance and dynamics in addition to generating realistic thermodynamic data, equipment design specifications and process efficiency prior to the practical implementation. This to a larger extent reduces commercialisation risk as production facilities are generally very difficult to modify once they have been implemented (Mohammed et al., 2019). The objective of this study was to evaluate the potentials of bioenergy production from millet chaff through comprehensive physicochemical evaluation, thermogravimetric analysis and combustion process simulation using Aspen Plus®.

2. Material and methods

2.1. Sample collection

Samples were collected manually from a static lot using a sampling scoop from a dump site in Bauchi state. Samples were taken from the top, middle and bottom of the material alternately. The samples as received had high moisture content and were sun pre-dried to avoid problems of decomposition by micro-organisms (BS EN 15442:2011). The material was ground to an average particle size of 1.0 mm and stored in air-tight plastic bags for further studies. Thereafter, the samples were sent for proximate, ultimate and thermogravimetric analyses at the Washington State University. The relatively small particle size of the biomass used in this study is to avoid heat transfer limitations during thermogravimetry studies, a phenomenon generally associated with larger sample size (Thoharudin et al., 2022).

2.2. Proximate and ultimate analyses

Proximate analysis was carried out to determine the moisture content, fixed carbon, volatiles, and ash content of the sample. This test was conducted in a thermogravimetric analyser (TGA) SDTA851e (Mettler Toledo, US). Known amount of sample was placed in a crucible, heated to 120 °C in the nitrogen atmosphere for 3 min and the moisture content was determined as the weight loss. The volatile matter was determined by heating the sample to 950 °C under nitrogen for 5 min and later cooled to 450°C. The volatile matter content was computed as the percentage weight difference before and after the heating. Ash content was determined as the remaining mass after the char was subsequently heated to 600°C and held for 8 min under oxygen flow (Ayiania et al., 2019). Ultimate analysis was performed using a TRUSPEC-CHN® (LECO, US) elemental analyser. Briefly, the instrument was calibrated as outlined in the instrument operating manual by running blanks and control samples for CHN. The calibration samples were wrapped and sealed in tin aluminium foil cups (LECO®) and fired at 950 °C in an ultra-high pure oxygen (99.993% purity) atmosphere using helium as a carrier gas for combustion products. This procedure was used for the biomass sample with approximately 0.15 g oven-dry sample. The experiment was repeated in triplicates for reproducibility. The oxygen (O) mass fraction was determined by difference (Pelaez-Samaniego et al., 2014). The structural analysis of the biomass was performed according to the procedure outlined in NREL/TP-510-42618. The inorganic composition analysis was conducted using an inductively coupled plasma mass spectrometer (ICP-MS Agilent 7500cx) instrument as outlined in Ayiania et al. (2019). Briefly, 100 mg sample was mixed with concentrated nitric acid (HNO_3:69–70%) (3 mL), followed by addition 2 mL hydrogen peroxide (H_2O_2: 30%) in a microwave digester (SP-D, CEM corporation) at 300°C and 250 psi for 5 min using a 5-min ramp to attain digestion conditions. Internal standard (Accustandard, Inc.) (1 mL) was added to each digested solution and subsequently diluted to 100 mL using deionised water. Argon was used as a carrier gas at 0.90 L/min and

0.25 L/min for the nebulizer and makeup respectively. Calibration graph was developed using a multi-element standard. The nature of chemical bonds and functional groups was evaluated by Fourier transform infrared spectroscopy (FTIR) on Agilent Cary 630 FTIR Spectrometer. About 2 mg homogenised samples were placed on the crystal surface at the centre (window) right above the hammer and subsequently, the hammer was closed to liquefy the crystal into a clear window to obtain the infrared (IR). The spectra were recorded with the Agilent MicroLab PC software within the wavenumber range of 400–4000 cm^{-1} at 140 scans and 4 cm^{-1} resolutions.

2.3. Thermogravimetric analysis (TGA)

Thermogravimetric analysis (TGA) was conducted in the oxygen atmosphere (20 mL/min) with the aid of simultaneous thermal analyser (TGA) SDTA851e (Mettler Toledo, US). The decomposition profile was evaluated from ambient temperature to 850°C at 5, 10 and 15°C/min heating rates. Sample size of approximately 7.0 mg (particle size of 0.2 mm) was used. The sample weight loss and derivative weight loss with respect to temperature were recorded simultaneously during the tests and used to produce the TG and DTG curves respectively.

2.4. Kinetics and thermodynamics

Kinetics of thermal decomposition of lignocellulosic materials have been studied using different models such as single step global model (SSGM), Flynn–Wall–Ozawa method (FWO) and Kissinger–Akahira–Sunose (KAS) (Islam et al., 2016) and distributed activation energy model (DAEM) (Mohammed et al., 2018a,b; Navarro et al., 2018; Szűcs et al., 2020; Yan et al., 2020). The DAEM is considered to be more accurate since it can mathematically represents the physical and chemical heterogeneity of the solid fuel (Várhegyi et al., 2002), thus widely used to model complex decomposition processes of lignocellulosic materials. It assumes that the decomposition process proceeds via several independent, parallel first-order reactions with each exhibiting individual frequency factor and activation energy. In addition, unlike other models, DAEM requires no mathematical model fitting to describe the kinetic parameters, instead a set of experimental data that relate weight loss to temperature/time at three different heating rates (Parthasarathy et al., 2021). It also suggested that at the same conversion rate (V/V*), the activation energy has a continuous distribution represented by a function f(E). All the parallel reactions are considered to be irreversible first-order with respect to the remaining volatile content and according to Miura and Maki (1998) is given by:

$$1-\frac{V}{V^*}=\int_0^{\infty} exp\left\{k_0\left(\int_0^t e^{-\left(\frac{E}{RT}\right)}dt\right)\right\}.f(E)dE \tag{1}$$

$$but\ \beta\ (heating\ rate)=\frac{dT}{dt}\ \Rightarrow dt=\frac{dT}{\beta}$$

Then Eq. (1) becomes:

$$1-\frac{V}{V^*}=\int_0^{\infty} exp\left\{\left(\frac{-k_0}{\beta}\right)\left(\int_0^T e^{-\left(\frac{E}{RT}\right)}dT\right)\right\}.f(E)dE \tag{2}$$

where V* is the effective volatile content, V is the volatile content at temperature T, β is the heating rate, k_0 is the pre-exponential factor, E is the activation energy and f(E) is the distribution function for activation energy and is given in normalised form as:

$$\int_0^{\infty} f(E)dE=1 \tag{3}$$

Let Ø be function of activation and temperature such that:

$$Ø\ (E,T)=exp\left\{\left(\frac{-k_0}{\beta}\right)\left(\int_0^T e^{-\left(\frac{E}{RT}\right)}dT\right)\right\} \tag{4}$$

Then, Eq. (2) becomes:

$$1-\frac{V}{V^*}=\int_0^{\infty} Ø\ (E,T).f(E)dE \tag{5}$$

From Eq. (4),

$$Ø\ (E,T)=exp\left\{\left(\frac{-k_0}{\beta}\right)\varphi\right\} \tag{6}$$

Where

$$\varphi=\int_0^T\left(e^{-\left(\frac{E}{RT}\right)}\right)dT \tag{7}$$

Integrating Eq. (7) gives:

$$\varphi=\int_0^T\left(e^{-\left(\frac{E}{RT}\right)}\right)dT=\frac{RT^2}{E}\ e^{-\left(\frac{E}{RT}\right)} \tag{8}$$

Substituting Eq. (8) in Eq. (6) we have:

$$Ø\ (E,T)=exp\left\{\left(\frac{-k_0}{\beta}\right)\frac{RT^2}{E}\ e^{-\left(\frac{E}{RT}\right)}\right\}=exp\left\{\left(\frac{-k_0RT^2}{\beta E}\right)e^{-\left(\frac{E}{RT}\right)}\right\} \tag{9}$$

Substitution of Eq. (9) and Eq. (3) in Eq. (2) gives:

$$\begin{aligned}1-\frac{V}{V^*}&=\int_0^{\infty} exp\left\{\left(\frac{-k_0}{\beta}\right)\left(\int_0^T e^{-\left(\frac{E}{RT}\right)}dT\right)\right\}.f(E)dE\\ 1-\frac{V}{V^*}&=\int_0^{\infty} exp\left\{\left(\frac{-k_0RT^2}{\beta E}\right)e^{-\left(\frac{E}{RT}\right)}\right\}.f(E)dE\ \cong exp\left\{\left(\frac{-k_0RT^2}{\beta E}\right)e^{-\left(\frac{E}{RT}\right)}\right\}\\ 1-\frac{V}{V^*}&\cong exp\left\{-\left(\frac{k_0RT^2}{\beta E}\right)e^{-\left(\frac{E}{RT}\right)}\right\}\end{aligned} \tag{10}$$

Replacing the V/V* by ΔV and ΔV* in the Eq. (10) above where ΔV and ΔV* is the number of volatiles evolved and the effective volatile content for a certain number of reactions. We have:

$$1-\frac{\Delta V}{\Delta V^*}=exp\left\{-\left(\frac{k_0RT^2}{\beta E}\right)e^{-\left(\frac{E}{RT}\right)}\right\} \tag{11}$$

Taking the natural logarithm of both sides of the Eq. (11) gives:

$$ln\left(1-\frac{\Delta V}{\Delta V^*}\right)=ln\left[exp\left\{-\left(\frac{k_0RT^2}{\beta E}\right)e^{-\left(\frac{E}{RT}\right)}\right\}\right]$$

$$ln\left(1-\frac{\Delta V}{\Delta V^*}\right)=-\left\{\left(\frac{k_0RT^2}{\beta E}\right)e^{-\left(\frac{E}{RT}\right)}\right\}$$

Taking the natural logarithm of both sides again:

$$\begin{aligned}ln\left[ln\left(1-\frac{\Delta V}{\Delta V^*}\right)\right]&=ln\left[-\left\{\left(\frac{k_0RT^2}{\beta E}\right)e^{-\left(\frac{E}{RT}\right)}\right\}\right]\\ ln\left[ln\left(1-\frac{\Delta V}{\Delta V^*}\right)\right]&=-ln\left\{\left(\frac{k_0RT^2}{\beta E}\right)e^{-\left(\frac{E}{RT}\right)}\right\}\\ ln\left[ln\left(1-\frac{\Delta V}{\Delta V^*}\right)\right]&=-\left\{ln\left(\frac{k_0RT^2}{\beta E}\right)-\left(\frac{E}{R}\right)\frac{1}{T}\right\}\\ ln\left[ln\left(1-\frac{\Delta V}{\Delta V^*}\right)\right]&=-ln\left(\frac{k_0R}{E}\right)-ln\left(\frac{T^2}{\beta}\right)+\left(\frac{E}{R}\right)\frac{1}{T}\\ ln\left[ln\left(1-\frac{\Delta V}{\Delta V^*}\right)\right]&=-ln\left(\frac{k_0R}{E}\right)+ln\left(\frac{\beta}{T^2}\right)+\left(\frac{E}{R}\right)\frac{1}{T}\\ ln\left(\frac{\beta}{T^2}\right)&=ln\left(\frac{k_0R}{E}\right)+ln\left[ln\left(1-\frac{\Delta V}{\Delta V^*}\right)\right]-\left(\frac{E}{R}\right)\frac{1}{T}\\ ln\left(\frac{\beta}{T^2}\right)&=ln\left(\frac{k_0R}{E}\right)-ln\left[-ln\left(1-\frac{\Delta V}{\Delta V^*}\right)\right]-\left(\frac{E}{R}\right)\frac{1}{T}\end{aligned} \tag{12}$$

Subsequently, Miura and Maki (1998) approximated $(1-\frac{\Delta V}{\Delta V^*})$ to be 0.58 and substituting into the equaton (12) gives: $ln(\frac{\beta}{T^2})=ln(\frac{k_0R}{E})-ln[-ln(0.58)]-(\frac{E}{R})\frac{1}{T}$

$$ln\left(\frac{\beta}{T^2}\right)=ln\left(\frac{k_0R}{E}\right)+0.6075-\left(\frac{E}{R}\right)\frac{1}{T} \tag{13}$$

Eq. (13) takes the form of a straight line and both E and k_0 we can be obtained from gradient and intercept by following the steps (i-iv) as summarised below:

(i) Establish a graph of conversion versus temperature using TGA data from at least three different heating rates.
(ii) Evaluate (β/T^2) at selected conversion from the relationship obtained in (i) above for the different heating rates.

(iii) Develop a graph of $\ln(\beta/T^2)$ with respect to (1/T) at the selected conversions and compute the activation energy and the pre-exponential factor from the gradient and intercept according to the Eq. (13).
(iv) Construct a graph of activation energy values obtained in (iii) above against the conversion and differentiate the model to obtain the distribution function for activation energy.

The frequency factor (pre-exponential factor) can be expressed as a function of activation energy according to Eq. (14) below:

$$k_0 = k_1 e^{k_2 E} \tag{14}$$

Where k_1 and k_2 are constants, depending on the reacting material. This equation can further be linearised to give Eq. (15), a straight-line relationship and the value of k_1 and k_2 can be obtained from slope and intercept.

$$ln(k_0) = ln(k_1) + k_2 E \tag{15}$$

Thermodynamic parameters such as change in enthalpy (ΔH), entropy (ΔS) and Gibbs free energy (ΔG) are generally computed using the activation energy, frequency factor and other constants like Boltzmann and Planks constants. According to Kim et al. (2010), these parameters can be computed using the following equations:

$$\Delta H = E_a - RT \tag{16}$$

$$\Delta G = E_a + RT_m ln\left(\frac{K_B T_m}{hA}\right) \tag{17}$$

$$\Delta S = \frac{\Delta H - \Delta G}{T_m} \tag{18}$$

Where K_B is the Boltzmann constant (1.83×10^{-23} J/ K), h is the Planck's constant (6.36×10^{-34} J.s), T_m is the peak temperature at maximum weight loss in the DTG curve.

2.5. Process model development

The combustion process coupled with power generation using millet chaff as a feedstock was first conceived in a Microsoft vision environment as shown in Fig. 1. The process is made up of two sections, the combustion section and power generation section. The former consists of a combustion reactor and solid-gas separation unit represented by a cyclone while the latter consists of a boiler, steam turbine, condenser and a pump. In the reactor, combustion reactions are effected and generates high temperature flue gas. The gas is generally accompanied with fine solid particles of inorganic components of the biomass feedstock, which is separated in the cyclone. The high temperature, solid-free flue gas is then charged into the boiler in the power generation section where it exchanges heat with water and generates high pressure steam. The steam is sent to the turbine for electricity generation while a lower pressure steam from the turbine is recirculated into the boiler via a condenser and pump.

3. Results and discussion

3.1. Physicochemical characteristics of millet chaff

Physicochemical characteristics of the biomass are summarised in Table 1. Proximate analysis results revealed that the millet chaff as received had moisture content of 7.9 wt% with ash content, fixed carbon and volatile matter (on dry basis) of 13.40, 15.35 and 71.25 wt% respectively, and higher heating value of 13.15 MJ/kg. These characteristics are similar to that of typical agro-residue biomass such as Almond shell, Nut shell (Ortiz et al., 2020), Bambara groundnut shell (BGS), oil palm fronds (OPF) peanut shell (PNS), and adzuki bean pods (AZP) as reported in the literature. Recent studies by Boubacar Laougé and Merdun (2020) on millet chaff (MCHF) reported ash content of 34.51 wt%, which is nearly three folds higher than the ash content recorded in the current study. This variation could be attributed to cultural practices during the crop cultivation and biomass pre-processing handling, since ash contents of biomass either originate directly from the fuel or incorporated during fuel handling (Mohammed et al., 2017a). The volatile matter of 71.25 wt% recorded is similar to that of BGS but 14% less than that of Napier grass (NG) and OPF, 7% lower with respect to that of AZP, and 8-14% higher than that of PNS and MCHF reported in the literature. This is an indication that the millet chaff biomass reported herein would be a suitable feedstock for the combustion process. A high volatile matter content biomass is generally characterised with rapid and difficult combustion, which mostly requires a bigger reactor volume to prevent high rate of pollutant emissions during the combustion (Adeleke et al., 2020). Boubacar Laougé and Merdun (2020) reported the heating value of MCHF with ash content of 34.51 wt% to be 17.53 MJ/kg compared to the 13.15 MJ/kg with ash content of 13.40 wt% recorded herein. This is contrary to the general trend as a higher ash content biomass is expected to have a lower calorific value. Compared with other agro-residues, the heating value of millet chaff recorded in this study is 25-51% lower than that of BGS, OPF, PNS, AZP and NG (Table 1). These differences could be mainly attributed to disparities in the ash content in addition to other physicochemical characteristics. The result of ultimate analysis indicated that the sample consists of 35.50 wt% carbon (C), 4.44 wt% hydrogen (H), 2.05 wt% nitrogen (N), 1.05 wt% sulphur (S) and 56.99 wt% oxygen (O). The ultanal attributes exhibited by the biomass is in consonant with the general trend of elemental composition of biomass. Fig. 2 shows the Van Krevelen plot of the millet chaff in comparison with another biomass. The H/C atomic ratio of the sample is similar to that of OPF, NG, PNS and MCHF. This characteristic signifies that the biomass may be energy efficient fuel. On the other hand, the O/C ratio of the sample was higher due to higher oxygen content, which is in good agreement with the lower magnitude of heating value recorded (Fantozzi and Bartocci, 2017). This further suggests that the sample will require a lower equivalence ratio during the thermochemical conversion compared to the other agro-residues (Ciuta et al., 2018), an indication of possible reduction of energy requirement of the thermochemical process.

The chemical composition such as the lignin and holocellulose (cellulose and hemicellulose) analysis results of the sample showed that holocellulose accounted for nearly 70% Table 1) while the lignin represents the remaining mass. The cellulose content (50.51 wt%) recorded is in good agreement with that of MCHF in the literature. Boubacar Laougé and Merdun (2020) reported 48.93 wt% cellulose, 3.16 wt% hemicellulose and 15.75 wt% lignin. The difference in the hemicellulose and lignin may be attributed to divergent environmental and cultivation conditions. Compared with other biomass material, the millet chaff in this study has 23% higher cellulose content than the NG biomass but comparable hemicellulose and lignin contents. The higher cellulose in the millet chaff could be responsible for the higher oxygen content which in turn affected the heating value (Nazli, 2020). Mineral composition analysis of the ash was conducted using inductively coupled plasma mass spectrometer and the result revealed the presence of sodium (Na), potassium (K), calcium (Ca), magnesium (Mg), iron (Fe) and aluminium (Al) (Table 1) as the major element in the following decreasing order of proportion: K>Al>Mg>Ca>Fe>Na. Elemental composition of biomass ash reported in the literature showed that K is mostly the dominant mineral component, which is consistent with the result recorded herein for the sample. The quantitative analysis of the minerals in the sample is critical for unknown fuel like millet chaff to predict possible operational challenges such as slagging, fouling and corrosion during combustion. Alkaline and alkaline earth metals particularly Na, K and Ca are generally released into the flue gas during combustion, which may lead to deposition on heat exchanger surfaces (Mlonka-Mędrala et al., 2020). Some empirical indicators such as slagging and fouling indices computed according to Eqs. (17–19) have been used to evaluate the biomass ash composition in order to predict its severity on the combustion process

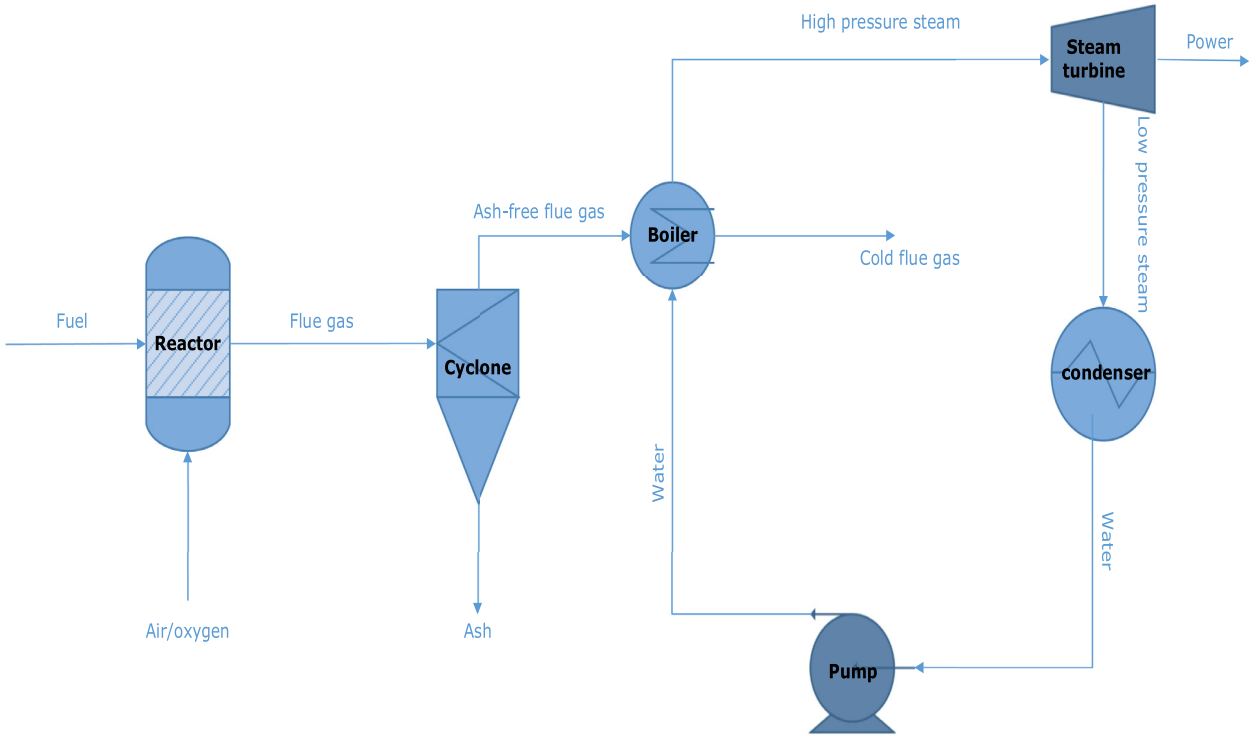

Fig. 1. Schematic conceptual process flowsheet of millet chaff combustion coupled with steam turbine for power generation.

Table 1
Average characteristics of Millet Chaff (°Present study; [1]Mohammed et al. 2015; [2]Mohammed et al. 2017; [3]Yakub et al. 2015; [4]Kuprianov and Arromdee, 2013; [5]Mohammed et al. 2018; [6]Boubacar Laougé and Merdun, 2020.

Property	Value						
Proximate analysis (wt%)	MCHF°	NG[1]	BGS[2]	OPF[3]	PNS[4]	AZP[5]	MCHF[6]
Moisture content	7.90±0.44	75.27±0.21		11.71			3.6
Ash content[a]	13.40±2.50	1.75±0.01	10.10±0.41	3.61	5.7	6.24 ± 1.21	34.51
Volatile matter[a]	71.25±2.12	81.51±0.30	73.83±1.39	80.88	65.4	76.10 ± 0.22	61.29
Fixed carbon[b]	15.35±0.38	16.74±0.09	16.08±0.71	15.51	19.6	17.66 ± 0.50	0.59
Heating value (MJ/kg)[a]	13.15±0.57	18.11±0.10	19.19±0.01	17.55	16.4	19.85 ± 0.01	17.53
Ultimate analysis (wt%)[a]							
Carbon (C)	35.50±1.30	48.61±0.80	34.63±0.92	45.05	56.59	39.41 ± 1.12	43.66
Hydrogen (H)	4.44±0.40	6.01±0.14	11.28±0.22	5.86	6.45	10.68 ± 0.15	6.3
Nitrogen (N)	2.02±0.10	0.99±0.03	1.16±0.04	0.23	1.53	2.95 ± 0.09	0.45
Sulphur (S)	1.05±0.00	0.32±0.01	1.00±0.01	0.04	0.09	0.93 ± 0.01	0.06
Oxygen (O)[c]	56.99±1.60	44.07±0.66	51.93±1.16	48.82	35.34	46.03 ± 1.10	49.54
Chemical composition (wt%)[d]							
Cellulose	50.51±2.61	38.75 ± 2.30	-	-	-	-	48.93
Hemicellulose	18.59±1.22	19.76 ± 1.68	-	-	-	-	3.16
Lignin	30.90±2.01	26.99 ± 1.29	-	-	-	-	15.75
Inorganic Mineral	***ICPMS (mg/g)***	***(EDX wt%)***					
Sodium (Na)	2.5±0.14	0.27±0.01	-	-	-	-	
Potassium (K)	67.49±0.13	64.77±2.23	72.57±2.10	50.22	9.34	73.06 ± 1.29	-
Calcium (Ca)	13.30±0.00	4.34±0.13	-	19.68	4.43	13.16 ± 0.02	-
Magnesium (Mg)	14.19±0.55	2.34±0.08	2.57±0.07	1.51	1.96	1.13 ± 0.07	-
Iron (Fe)	11.45±0.71	-	-	-	8.11	1.52 ± 0.02	-
Aluminum (Al)	22.56±0.00	0.93±0.03	4.15±0.11	0.64	11.6	2.53 ± 0.10	-

[a] Dry basis
[b] by difference [100- (Ash+Volatile matter)]
[c] by difference [O=100 - (C + H + N + S)]
[d] extractive and ash free basis

(Wang et al., 2017).

$$Base/acid\ ratio\ (R_{B/A}) = \frac{Fe_2O_3 + CaO + MgO + K_2O + Na_2O}{SiO_2 + TiO_2 + Al_2O_3} \quad (17a)$$

$$Slagging\ index\ (SI) = (R_{B/A}) \times S \quad (18a)$$

$$Fouling\ index\ (FI) = (R_{B/A}) \times (K_2O + Na_2O) \quad (19)$$

Where S is the sulphur content.

From Table 1, using appropriate conversion factors as outlined in the British standards BS EN 15290:2011) to obtain the oxide form of the elements, the millet chaff ash slagging and fouling index recorded was 3.52 and 282.64 respectively. This suggests that the sample has extremely high slagging inclination (>2.6) and extremely high fouling indication (>40). Considering the Eqs. (17) and ((19), the major contrib-

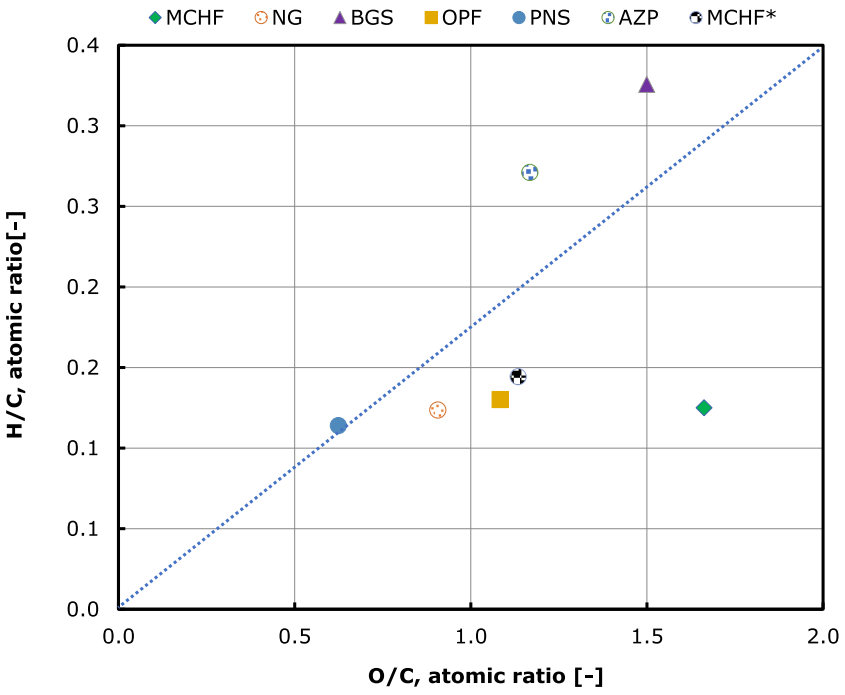

Fig. 2. Van Krevelen diagram of millet chaff.

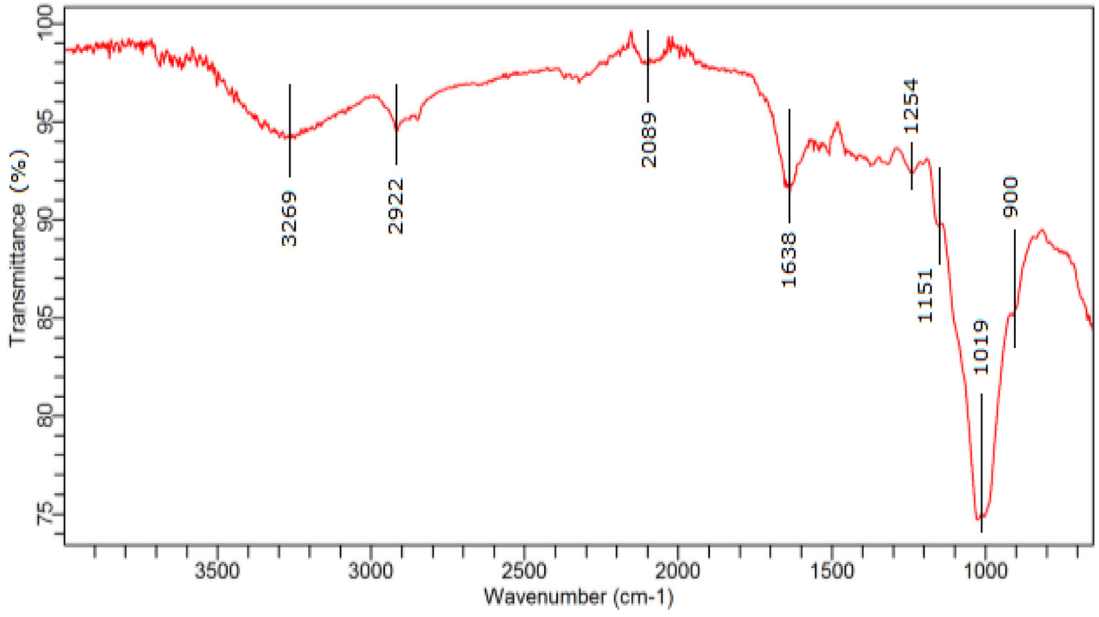

Fig. 3. Averaged FTIR spectrum of millet chaff sample.

utors are the CaO, MgO, K_2O and Na_2O. These components are soluble in water and could be leached out easily. According to Mohammed et al. (2017a), 74-90% of Na_2O and K_2O could be leached out with water at room temperature in addition to significant reduction of CaO and MgO at pre-treatment severity of 2.7, which corresponds to 6 hrs leaching operation. Under this condition, the indices of the resulting sample will drop from the extreme conditions to medium slagging inclination and high fouling indication, which is considerable for the combustion process. Consequently, aqueous pre-treatment of millet chaff with water is necessary prior to its utilisation as fuel in the combustion process.

Functional group analysis of the sample was performed using Fourier transformed infrared (FTIR). Accordingly, the FTIR spectrum of chemical species in the millet chaff sample is shown in Fig. 3. The sample exhibited peaks at 3269 cm^{-1}, which is ascribed to different hydroxyl groups $(O-H)$ corresponding to mostly alcohol and phenolic compounds in the sample. While the peak at 2922 cm^{-1} is due to aliphatic saturated $C-H$ stretching vibrations of methylene group probably from lignin components of the biomass (Sajjad Ahmad et al., 2020). The peak at a frequency around 2089 cm^{-1} is ascribed to $C \equiv C$ functional group (Mohammed et al., 2017c). The band at 1638 cm^{-1} is due to ring conjugated $C=C$ bonds of lignin while the ones at frequency of 1254 and 1151 cm^{-1} correspond to $O-H$ bending in holocellulose (Mohammed et al., 2015). The wave number 1019 cm^{-1} is ascribed to $C-O$ mainly in the cellulose and hemicellulose while the fingerprint at 900 cm^{-1} is attributed to aromatic $C-H$ bending vibrations due to the presence of lignin in the samples (Reza et al., 2020). Therefore, the

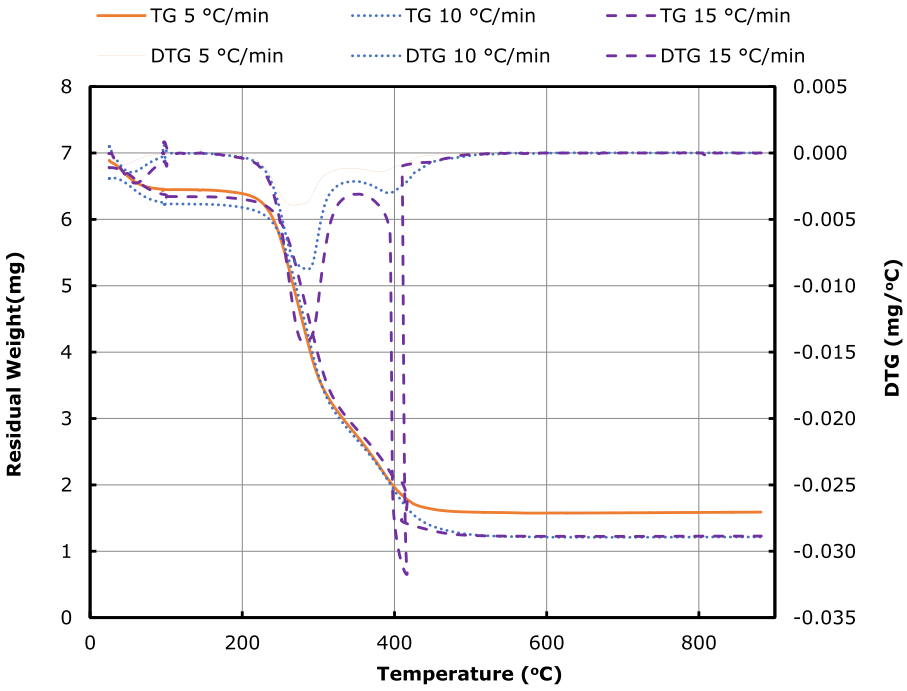

Fig. 4. Thermogravimetric profile of millet chaff under oxygen atmosphere.

FTIR result indicates the presence of hemicellulose, cellulose and lignin in the sample, which is in good agreement with the chemical composition analysis result.

3.2. TG and DTG profile of millet chaff

TGA characteristics of millet chaff under oxygen atmosphere at three different heating rates is shown in Fig. 4. The combustion process proceeded in three stages. In stage one, two distinct regions were identified. At temperatures under 90 ^{0}C, a visible shoulder on the derivative thermogravimetry (DTG) for all the heating rates were observed. This represents the initial evolution of moisture, which accounts for about 6% weight loss. The second region under the stage one signifies further drying of the sample and devolatilisation of some very light components at 96.25-189.65 ^{0}C, 107.07-192.36 ^{0}C and 121.05-197.43 ^{0}C for 5 ^{0}C/min, 10 ^{0}C/min and 15 ^{0}C/min respectively with corresponding weight loss of 0.78 wt%, 0.64 wt% and 0.55 wt%. The total weight loss recorded for the individual heating rate is 6.78 wt%, 6.64 wt% and 6.55 wt% as summarised in Table 3. The stage two constitutes thermal degradation of hemicellulose, cellulose and lignin in the biomass through sequence of chemical reactions such as volatiles emission, volatiles ignition, volatiles burning into flames and volatile flame extinction. These chemical reactions were observed at 204.00-322.54 ^{0}C, 217.05-324.46 ^{0}C and 222.30-348.68 ^{0}C with respect to 5 ^{0}C/min, 10 ^{0}C/min and 15 ^{0}C/min heating rate. The corresponding weight loss noted from the TG curve was 50.63 wt%, 50.65 wt% and 54.19 wt%. Comparing with the literature, it has been reported that decomposition temperature of hemicellulose, cellulose and lignin under an oxidised atmosphere to be within 220–315°C, 315–400°C and 175–890°C respectively (Bi et al., 2020). This suggests that the identified temperature range for the chemical reaction fully covered the decomposition temperature of hemicellulose and therefore, the weight loss noted can be attributed to full thermal breakdown of hemicellulose and transformation of cellulose and lignin into residual carbon. The DTG curves under the stage two showed a broad peak with maximum reaction intensity of -0.005 mg/^{0}C, -0.009 mg/^{0}C and -0.014 mg/^{0}C at 269.81 ^{0}C, 279.84 ^{0}C and 285.18 ^{0}C corresponding to 5 ^{0}C/min, 10 ^{0}C/min and 15 ^{0}C/min heating rate. This trend shows that increasing the heating rate at intervals of 5 ^{0}C/min led to decline in the reaction intensity by more than 50%, suggesting an inverse relationship between the heating rate and the weight loss rate. The higher reaction intensity (-0.005 mg/^{0}C) characterised by lower peak temperature recorded at 5 ^{0}C/min signifies faster combustion reactions (Ahn et al., 2020) due to efficient heat transfer between the individual biomass particles. This observation is similar to the findings reported by Boubacar Laougé and Merdun (2020). The authors recorded maximum weight loss rate at lower temperature under lower heating rates, which was attributed to efficient heat transfer between the biomass particles. Similarly, Islam et al. (2016) reported that lower heating rates provide adequate residence time for heat to permeate steadily into the biomass particles, which give rise to effective heat transfer between the particles. Stage three represents the oxidation of residual cellulose and lignin, and the resulting carbonaceous material with a peak observed at 347.29-423.21 ^{0}C, 363.28-426.27 ^{0}C and 401.76-431.50 ^{0}C corresponding to 5 ^{0}C/min, 10 ^{0}C/min and 15 ^{0}C/min heating rate. With increasing heating rate, the fairly broad peak shrinks to a sharp peak, indicating the overlapping of the oxidation phase of carbon residues from both cellulose and lignin (Maia et al., 2020). From the TG curve, 37.55, 38.65 and 35.55 wt% were recorded with respect to 5 ^{0}C/min, 10 ^{0}C/min and 15 ^{0}C/min heating rate (Table 3). The corresponding reaction intensity was -0.0014 mg/^{0}C, -0.003 mg/^{0}C and -0.032 mg/^{0}C and maximum peak temperature of 381.95 ^{0}C, 396.92 ^{0}C and 416.39 ^{0}C. The lower peak temperature (381.95 ^{0}C) and the DTG value (-0.0014 mg/^{0}C) recorded at 5 ^{0}C/min shows that the combustion of carbon residues is accomplished faster at lower heating rate with higher reaction intensity (Chen et al., 2020). Comparing this reaction intensity with that recorded in the stage 2 (-0.005 mg/^{0}C) at 5 ^{0}C/min, it revealed that the combustion of residual carbon proceeded faster relative to that of stage 2, which suggests a lower energy barrier for the reaction progression. This is also true for the other heating rates except that observed at 15 ^{0}C/min, where the combustion of residual carbon recorded lower intensity, which could be attributed to complex decomposition pathways due to rapid heating cum the catalytic effect of the minerals present in the ash. This is in good agreement with the findings reported by Chen et al. (2020). The authors stated that the inorganic components in biomass ash particularly the alkali and alkaline earth metals are active in catalysing char combustion reaction. Considering the overall weight loss for the entire combustion process on dry basis, the average weight loss recorded was 89.07±0.80 wt% while the remaining mass (10.93±1.57 wt%) represents the non-

combustible materials, which is comparable with the ash content earlier obtained in the proximate analysis.

3.3. Ignition and burnout temperatures of millet chaff

Combustion behaviour of fuel is generally characterised by two key parameters such as ignition temperature and burnout temperature. Ignition temperature (T_{ign}) is the least temperature when the combustion reaction of the fuel becomes self-sustaining. It can also be defined in terms of fuel safety and storage as the lowest possible temperature at which a fuel ignites freely in an environment devoid of external source of ignition. While the burnout temperature (T_{bnt}) is the temperature at which the fuel is entirely exhausted (Lu and Chen, 2015). These thermal properties can be evaluated from the TG and DTG profile of the fuel. Determination of T_{ign} of biomass sample is carried out using intersection method and deviation method. The intersection method is accomplished by using a vertical line (VL_1) through the DTG peak and a tangential line (TL_1) on the TG curve where the vertical line intersects (W). With another line (HL_1) parallel to x-axis on the TG curve during the constant weight before the decomposition begins, ignition temperature is the temperature at the point of intersection (X) between the TL_1 and HL_1 on the TG curve (Ahn et al., 2020; Guo et al., 2020) as shown in Fig. 5a. The deviation method of establishing T_{ign} involves comparing the DTG curves under inert and oxidised atmospheres and T_{ign} is the point at which the disparity between the two DTG curves approaches 3% (Lu and Chen, 2015; Maia et al., 2020) as presented in the Fig. 5b. Similarly, the T_{bnt} is evaluated from the TG and DTG profile of the fuel using the intersection method and conversion method. Consider Fig. 5a also, the T_{bnt} following the intersection approach is obtained from the char decomposition peak instead of the volatile decomposition peak (first peak). In a similar manner to the determination of T_{ign}, a vertical line (VL_2) through the second DTG peak and a tangential line (TL_2) on the TG curve are drowned and intersect at point (Y). With another horizontal line (HL_2) drawn parallel to abscissa on the TG curve after the char decomposition with nearly zero weight loss, T_{bnt} is the temperature at the point of intersection (Z) between the TL_2 and HL_2 on the TG curve. On the other hand, T_{bnt} by conversion method is the temperature at which the conversion of fuel reaches 99% (Lu and Chen, 2015). Accordingly, the T_{ign} recorded for the sample was 232.94 ^{0}C, 240.75 ^{0}C and 244.27 ^{0}C (Table 4) at 5 ^{0}C/min, 10 ^{0}C/min and 15 ^{0}C/min respectively following the intersection method while the values recorded through the deviation method was 220.33 ^{0}C, 223.83 ^{0}C and 231.25 ^{0}C. The values of T_{ign} recorded through the deviation method are 5-7% lower relative to the T_{ign} values obtained from the intersection method. Increase in the heating rate increased the T_{ign} values from both methods. This trend could be linked to inefficient heat transfer within the individual particle and between the particles as rapid heating generates temperature lag between the particle surface and the core. Similar observations have been reported in the literature. According to Liu et al. (2019), higher heating rates promotes rise in the decomposition temperature of organic matter, which induces temperature difference between the inside and outside of biomass particles. Maia et al. (2020) also noted variation in the ignition, which was directly linked to the heating rates. Considering the decomposition temperature of the biomass components under the oxidised environment, all the T_{ign} values obtained from both methods are within the decomposition temperature of hemicellulose. Consequently, the ignition temperatures of millet chaff evaluated from the intersection and deviation methods are principally from hemicellulose decomposition reaction due to its higher reactivity compared to the cellulose and lignin. The T_{bnt} noted from the intersection method was 429.56 ^{0}C, 451.91 ^{0}C and 462.59 ^{0}C at 5 ^{0}C/min, 10 ^{0}C/min and 15 ^{0}C/min (4) compared to 446.43 ^{0}C, 460.18 ^{0}C and 489.06 ^{0}C obtained using the conversion method. The observed values of T_{bnt} from both methods are also shifted to higher temperature regions with increasing heating rates. This is attributed to the heat transfer limitation propagated by faster heating rates, which prolong completion of combustion reaction. The T_{bnt} values are in reasonable agreement within 1.8-5.7 deviation. Therefore, both intersection and conversion methods could be applied in determining the burnout temperature of biomass fuel. According to literature, the ignition and burnout temperatures of other lignocellulosic materials and agro-residues in oxidised atmospheres are between 245–268 ˚C and 466–596 ˚C respectively (Liu et al., 2019). These values are somewhat comparable with the thermal characteristics of millet chaff recorded herein. The lower value of ignition temperatures of millet chaff relative to other biomass materials is attributed to dissimilar physicochemical properties such as volatile matter, ash content and chemical composition (hemicellulose, cellulose and lignin) in addition to disparity in the operating conditions.

3.4. Combustion kinetic parameters

The degree of conversion of millet chaff in the oxidised atmosphere at different heating rates with respect to temperature is shown in Fig. 6. It can be seen that the combustion process of the sample could be defined (on a dry basis) at a conversion value between 10% and 90% with the corresponding temperatures represented as T_{10} and T_{90}. At 5 ^{0}C/min, the T_{10} recorded was 209.42 ^{0}C compared to 226.77 ^{0}C observed for both 10 ^{0}C/min and 15 ^{0}C/min. Conversion degree of 50% was achieved at T_{50} value of 284.10 ^{0}C, 293.93 ^{0}C and 298.52 ^{0}C with respect to 5 ^{0}C/min, 10 ^{0}C/min and 15 ^{0}C/min while the corresponding T_{90} was 389.69 ^{0}C, 409.78 ^{0}C and 416.61 ^{0}C. The value of T_{10} recorded at 5 ^{0}C/min is below the T_{ign} (232.94 ^{0}C /220.33 ^{0}C) earlier observed (Table 4), suggesting the combustion mechanism could be mainly volatile emission while the T_{10} obtained for 10 ^{0}C/min and 15 ^{0}C/min is within the observed T_{ign} values, which possibly indicates simultaneous volatile emission and volatile ignition. The conceivable mechanisms towards 50% degree of conversion could be volatile ignition and volatile burning into flame for 5 ^{0}C/min while only volatile burning into flame possibly dominates for 10 ^{0}C/min and 15 ^{0}C/min. The value of T_{70} recorded (Fig. 6) for all the heating rates is within 320-346 ^{0}C, which agrees with the end point of stage II earlier identified (Table 3). This implies that flame extinction is probably the main pathway at 50-70% degree of conversion. While the decomposition of residual carbon is highly likely at a degree of conversion above 70%. Conversion of millet chaff with possible combustion mechanisms are summarised in Table 5. Fig. 7 shows the millet chaff combustion linear plot developed from $\ln(\beta/T^2)$ with respect to (1/T) at the selected conversions according to the Eq. (13). Imaginary lines through the points at each of the heating rates showed a parallel relationship, suggesting equal gradient and similar characteristics. A linear fit to the set of three different heating rates with the same conversion exhibited a very good relationship between $\ln(\beta/T^2)$ and (1/T) with R-squared value of 0.82-0.99 (Table 6). Gradient and intercept of the linear fit is used for computation of activation energy and the pre-exponential factor. Accordingly, the trend of activation energy of millet chaff combustion at various conversions showed five (A-E) distinct regions (Fig. 8). At conversion between 0.1-0.2 (stage A), a direct positive relationship is observed, an indication of similar activities/mechanisms. The corresponding activation energy changed from 91.95 kJ/mol to 164.44 kJ/mol, probably due to increasing activation of molecules for chemical reaction. According to Barzegar et al. (2020), during biomass combustion, activation energy values of around 175 kJ/mol is as a result of hemicellulose decomposition, usually within 10-20% degree of conversion. Between 0.2 and 0.5 conversion (stage B), a second positive correlation is also observed and the change in activation energy was 164.44-189.55 kJ/mol. The raise in the value of activation energy is not as rapid as in the earlier stage, which connotes larger reaction barrier attributed to multiple reaction steps with probable interactions between the intermediates from different pathways resulting from decomposition of the remaining hemicellulose and commencement of full breakdown of cellulose and lighter parts of the lignin. In addition, biomass cellulose consists of amorphous and crystalline components. The latter has higher

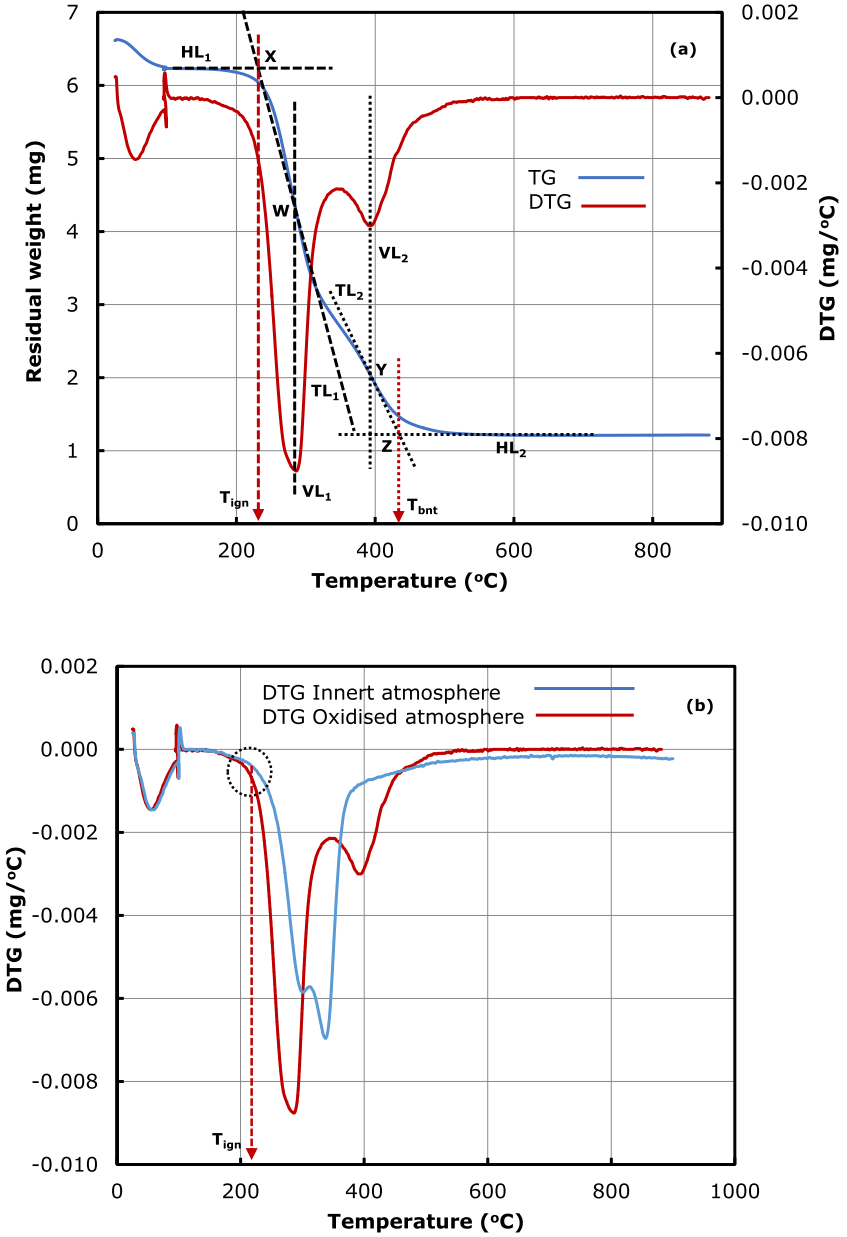

Fig. 5. TG and DTG profile of millet chaff for determination of thermal properties (a) ignition temperature (T_{ign}) and burnout temperature (T_{bnt}) using intersection method (b) ignition temperature using deviation method.

thermal stability (Chen et al., 2020), which may have contributed to higher values of the observed activation energy. The activation energy values recorded under this conversion range is similar to that reported in the literature, which was mainly attributed to cellulose degradation (Barzegar et al., 2020). Though, combustion of lignocellulosic material proceeds with overlapping multiple components degradation particularly at higher heating rate as rightly noted in the TGA analysis in the previous sections. At 0.5 conversion (stage C), a plateau is observed in the activation energy distribution profile of the sample, which can be regarded as a transition state where molecules exist neither as reactants nor final products, but as a chemical intermediate (activated complex). At this stage, more fuel consumption is expected, and the combustion reaction is fully developed. This observation strongly agrees with the proposed combustion mechanism of volatile burning into flame. A declining trend in the activation energy value (189.55 kJ/mol to 116.88 kJ/mol) is observed at conversion beyond 0.5 until 0.7 (stage D), this is probably due to decrease in the residual volatile content of the fuel, particularly from the cellulose and lignin, which became exhausted at the conversion of 0.7. Barzegar et al. (2020) reported that biomass decomposition in oxidised atmosphere at conversion between 0.5 and 0.7 results in decrease in the activation energy value down to nearly 90 kJ/mol, which was attributed to lignin degradation. Studies on combustion of lignin reported by Jianfei et al. (2020) also revealed lower activation energy in the range of 60.02–73.42 kJ/mol. These lower values of activation energy reported for lignin combustion compared to holocellulose combustion suggests that lignin combustion reaction progresses faster. In addition, the lignin degradation stage represents the single longest activation energy distribution (Fig. 8), which is corroborated with the long tailing observed in the DTG profile of the sample. This observation further suggests that the main combustion reaction in this stage is probably flame extinction, a sustained combustion stage that results in a quasi-steady vaporisation without any visible flame detected. This stage is generally accompanied with cool flame combustion characterised with many flame regimes and dynamics (Cuoci et al., 2017). The activation energy distribution pattern exhibited in stage E (Fig. 8) between 0.7 and 0.9 degree of conversion represents residual char combustion process. Under this regime, the activation energy value changed from 117 kJ/mol through 115 kJ/mol to 138 kJ/mol. According to Zou et al.

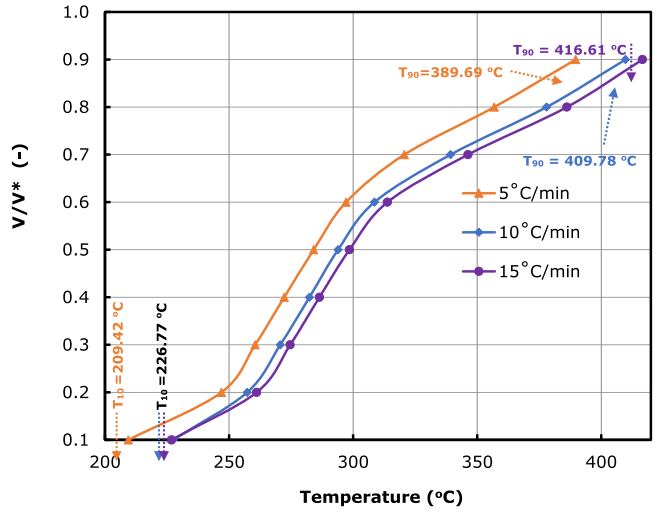

Fig. 6. Conversion of millet chaff versus temperature at different heating rate.

(2020), catalytic activities of mineral elements in the biomass control the decomposition reaction in the last phase of combustion process. It was reported that CaO promotes formation of complexes, which hindered the combustion reaction while Fe_2O_3 on the other hand favours the reaction. Consequently, the irregular trend observed in the activation energy value signifies a complex decomposition process, which can be attributed to the catalytic activities of the mineral elements present in the source biomass (Table 1). This observation is in line with the proposed residual carbon oxidation mechanism as stated in Table 5.

The distribution function *f*(E) of activation energy obtained from the derivative of the conversion versus activation energy is shown in Fig. 9. The distribution function exhibited two visible peaks within the activation energy range of 91.95-116.88 kJ/mol and 171-189.55 kJ/mol. This can be linked to the chemical composition of the biomass sample, which is in good agreement with the DTG profile of the sample. Similar observations have been reported in the literature. Fang et al. (2018) reported distribution function of activation energy with two visible peaks for a catalytic thermochemical decomposition of biomass samples. The authors attributed this pattern to the nature of chemical composition in the biomass sample. The pre-exponential factor (k_0), which is the frequency of collisions between molecules during the combustion is summarised in Table 6. The k_0 values exhibited two lower extremes with values within 10^{10} -10^{11} corresponding to 0.1, and 0.7-0.9 conversion and a central zone, having k_0 values between 10^{16} and 10^{18} under 0.2-0.6 conversion. The lower values of k_0 recorded suggests low reaction barrier, low molecular collision and easier conversion whereas the higher k_0 values signifies more heat requirement for higher molecular collision to be transferred and higher energy barrier to be overcome for the reaction to progress. These observations are strongly in good agreement with the observed activation energy values. Fong et al. (2019) reported that k_0 values within 10^9 is due to limitation in particle rotation of the activated complex relative to the initial reagent, which indicates a large surface reaction while k_0 values above 10^9 signifies no changes during the rotation of the active complex and reagent in the reaction. Recent reports by Boubacar Laougé and Merdun (2020) on combustion of millet chaff indicate k_0 values within 10^2-10^4, which is far below 10^9, suggesting a major limitation in particle rotation of the activated complex during the combustion process. Fig. 10 shows $\ln k_0$ versus activation energy relationship, which represents a linear fit for the compensation effects between k_0 and activation energy. The graph showed a positive linear relationship (R^2=0.9015) between the $\ln k_0$ and activation energy in accordance with the Eq. (15) above. The value of k_1 and k_2 obtained from the slope and intercept is 0.0041 and 0.2645 and the final relationship between k_0 and activation energy is represented in the form Eq. (14) below:

$$k_0 = 0.0041e^{0.2645E}$$

This equation indicates a minimal compensation effect since there is relatively no increase in the k_0 value at specific conversion with respect to activation energy. This could be attributed to the slow heating rates applied during the thermogravimetric analysis of the samples (Boubacar Laougé and Merdun, 2020; Mohammed et al., 2017b; Mohammed et al., 2018b).

3.5. Combustion thermodynamic parameters

The thermodynamic parameters (change in enthalpy-ΔH, entropy-ΔS and Gibbs free energy- ΔG) evaluated for the combustion of millet

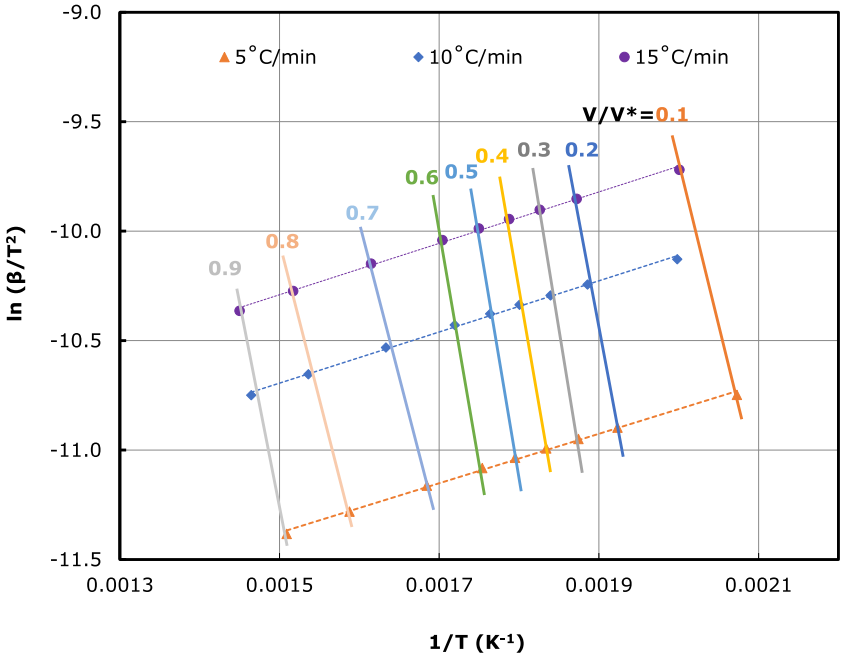

Fig. 7. Millet chaff combustion linear plot at different conversion and heating rate.

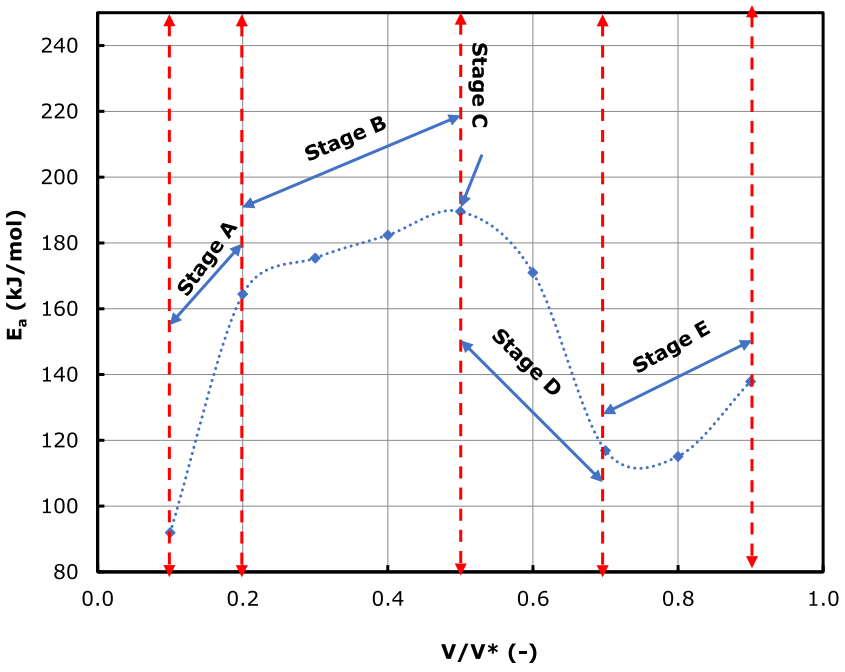

Fig. 8. Plot of activation energy distribution against degree of conversion for combustion of millet chaff.

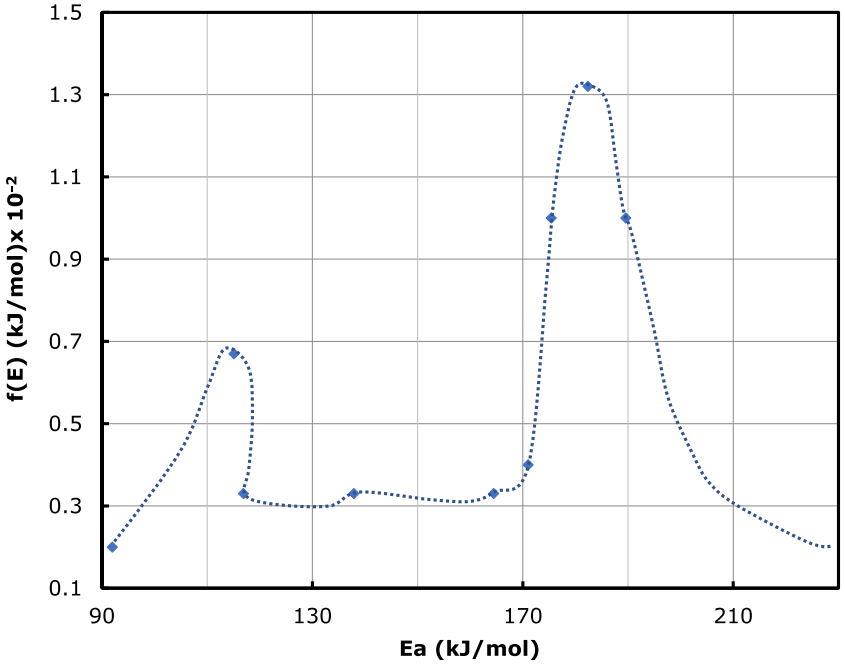

Fig. 9. Distribution func6tion f(E) of activation energy versus activation energy (E_a).

chaff are summarised in Table 6. The enthalpy change is the energy released during combustion. It also provides details of which part of the biomass releases the most energy during the combustion. The ΔH values recorded in this study increased with conversion. At low conversion (≤0.1), ΔH value was 87.31 kJ/mol, which doubled as the conversion increased from 0.2-0.6. This suggests that conversion of the most energy carriers within the biomass is achieved in this range. This is in good agreement with our earlier observation that suggested conversion of residual hemicellulose, full breakdown of cellulose and some parts of the lignin under similar conversion range. In addition, the trend exhibited by the ΔH is similar to that of the activation energy with a difference of approximately 5.0 kJ/mol for all conversions. This indicates the feasibility of combustion reaction since a large difference connote unlikeliness of the reaction (Ashraf et al., 2021; Boubacar Laougé and Merdun, 2020; Fong et al., 2019). The positive values of ΔH recorded implies that external heat is required to generate the activated complex during the combustion (Xu et al.). The entropy change (ΔS) describes the course of a process, whether it proceeds spontaneously and has a probability of occurring in a defined direction, or non-spontaneously and does not proceed in the defined direction, but in the reverse direction. The ΔS for the millet chaff combustion showed positive values of lower magnitude at conversion 0.1, 0.7,0.8 and 0.9. This infers that at these conversions, the sample is much away from thermodynamic equilibrium, which may further result in reactivity to produce activated complex within short reaction time. The low ΔS values indicate that the material just experienced some changes which brings it to a state close to its thermodynamic equilibrium. On the other hand, negative values were recorded for ΔS at conversion between 0.2-0.6, signifies that the activated complex is char-

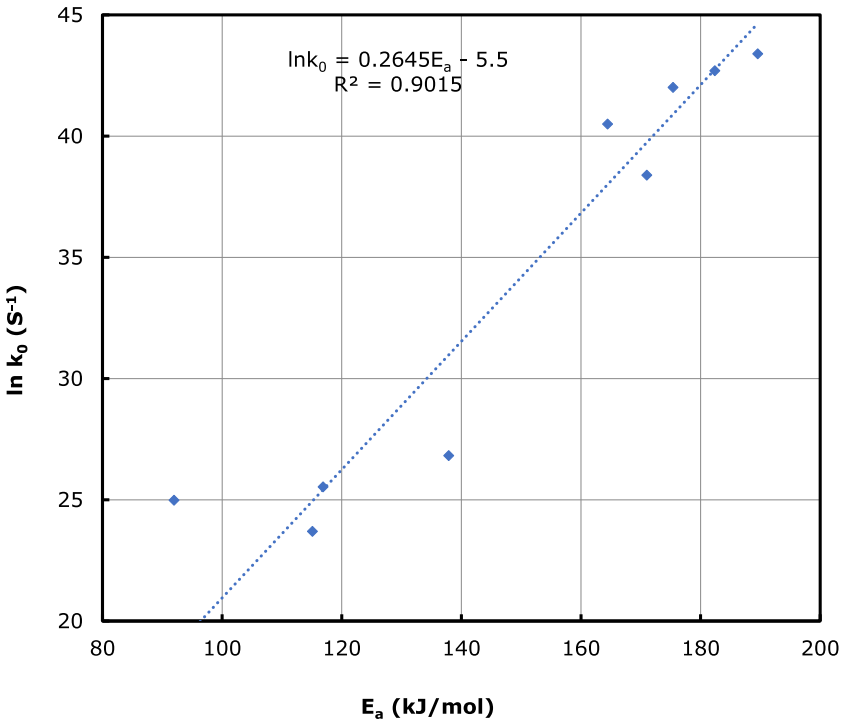

Fig. 10. Relationship between K_0 and Activation Energy (Ea).

acterised with high degree of arrangement and that the substance has just passed through some of the chemical process far from its thermodynamic equilibrium (Açıkalın and Gözke, 2021). These observations are in good agreement with the activation energy, frequency factor patterns and the proposed mechanisms that suggested volatile burning to flame extinction at 0.2-0.6 conversion. Similarly, combustion studies of millet chaff reported by Boubacar Laougé and Merdun (2020) also showed negative values of ΔS and were attributed to lower degree of disorder products relative to the source biomass. Similar observations have also been reported in the literature (Xu and Chen, 2013). The Gibbs free energy change (ΔG) connotes the total energy change during the combustion reaction, which can be used to adjudge the reaction pathways. The ΔG values recorded for the millet chaff spanned between 67 and 250 kJ/mol. Higher values above 200 kJ/mol were observed at 0.2-0.6 conversion, which can be attributed to high level of reactivity (Karuppasamy Vikraman et al., 2021) while the lower values recorded at 0.1, 0.7-0.9 conversions connote low reactivity (Açıkalın and Gözke, 2021).

3.6. Process model implementation in Aspen Plus

The combustion process was implemented in ASPEN PLUS® V11 software. The process flow diagram was developed with non-random two-liquid (NRTL) thermodynamic property data based on the assumptions that the average composition of Millet chaff is according to the physicochemical analysis (proximate and ultimate) as summarised in Table 1. Details of components used in the simulation from the Aspen property environment are outlined in Table 2. In the combustion section, the combustor is represented by two reactors (RYield and RGibbs) and a flue gas cleaning unit (cyclone). The RYield block is used to simulate initial combustion steps of the biomass such as the release of light volatile and decomposition into cellulose, hemicellulose, lignin and mineral composition (ash) as specified in the Table 1. The RGibbs reactor is based on the phase equilibrium and chemical equilibrium calculations through minimisation of Gibbs free energy of the system using the rigorous calculation option in the Aspen. Water vapor (H_2O), hydrogen (H_2), nitrogen (N_2), oxygen (O_2), sulphur dioxide (SO_2), sulphur trioxide (SO_3), nitric oxide (NO), nitrogen dioxide (NO_2), nitrous oxide (N_2O), carbon monoxide (CO) and carbon dioxide (CO_2) were selected as the expected components at equilibrium. The inorganic components were treated as pure solid in the combustion product stream (flue gas). Cyclone (CYCL) was implemented in the Aspen environment using the modified Leith-Licht method (Clift et al., 1991) at 95% separation efficiency. The power generation section on the other hand, was implemented using a flue gas heat exchanger (FGHX), steam turbine (S-TURBIN), condenser (W-COND) and a pump (W-PUMP). The combination of these units represents a typical steam turbine for combined heat and power (CHP), which operates on the Rankine cycle. Water (CWTER) is pumped with high pressure into FGHX and exchanged

Table 2
List of components used in the simulation.

Component ID	Type	Component name	Alias
WATER	Conventional	Water	H_2O
MCHF	Nonconventional	Millet Chaff	
SULFU-01	Conventional	Sulphur	S
NITRO-01	Conventional	Nitrogen	N_2
OXYGE-01	Conventional	Oxygen	O_2
SULFU-02	Conventional	Sulphur-dioxide	SO_2
SULFU-03	Conventional	Sulphur-trioxide	SO_3
NITRI-01	Conventional	Nitric-oxide	NO
NITRO-02	Conventional	Nitrogen-dioxide	NO_2
HYDRO-01	Conventional	Hydrogen	H_2
METHA-01	Conventional	Methane	CH_4
CARBO-01	Conventional	Carbon-monoxide	CO
CARBO-02	Conventional	Carbon-dioxide	CO_2
CARBO-03	Solid	Carbon-graphite	C
CELLU	Solid	Dilactic-acid	$C_6H_{10}O_5$
HCELL	Solid	Glutaric-acid	$C_5H_8O_4$
LIG-H	Solid	Ethyl-benzoate	$C_9H_{10}O_2$
LIG-G	Solid	Propyl-p-hydroxybenzoate	$C_{10}H_{12}O_3$
LIG-S	Solid	C11h14o4	$C_{11}H_{14}O_4$
POTAS-01	Solid	Potassium	K
CALCI-01	Solid	Calcium	Ca
MAGNE-01	Solid	Magnesium	Mg
ALUMI-01	Solid	Aluminium	Al
IRON	Solid	Iron	Fe
SODIU-01	Solid	Sodium	Na
NITRO-03	Conventional	DCS	N_2O

Table 3
Combustion characteristics of Millet Chaff at different heating rates.

β (°C/min)	Temperature intervals (°C)			weight loss intervals (wt%)			DTG_{max} (mg/°C)	T_{max} (°C)	DTG_{max} (mg/°C)	T_{max} (°C)
	stage I	stage II	stage III	stage I	stage II	stage III	stage II		stage III	
5	96.25-189.65	204.00-322.54	347.29-423.21	6.78	50.63	37.55	-0.005	269.81	-0.0014	381.95
10	107.07-192.36	217.05-324.46	363.28-426.27	6.64	50.65	38.65	-0.009	279.84	-0.0030	396.92
15	121.05-197.43	222.30-348.68	401.76-431.50	6.55	54.19	35.55	-0.014	285.18	-0.0320	416.39

Table 4
Ignition and burnout temperatures of millet chaff.

β (°C/min)	$T_{IGNITION}$ (°C)		$T_{BURNOUT}$ (°C)	
	Intersection method	Deviation method	Intersection method	Conversion method
5	232.94	220.33	429.56	446.00
10	240.75	223.83	451.91	460.18
15	244.27	231.25	462.59	489.06

Table 5
Possible combustion reaction pathways with respect to heating rates at different conversion.

Heating rate (°C/min)	Degree of conversion (DoC)	Possible Reaction Mechanism
≤ 5	≤10%	Volatile emission
≥ 10		Simultaneous volatile emission and volatile ignition
≤ 5	<10% DoC ≤50%	Volatile ignition and volatile burning into flame
≥ 10		Volatile burning into flame
5, 10 and 15	≤ 50% DoC ≤70%	Flame extinction
5, 10 and 15	>70%	Oxidation of residual carbon

Table 6
Kinetics and thermodynamic parameters of millet chaff combustion.

V/V*	E (kJ/mol)	R^2	k_o (s^{-1})	ΔH (kJ/mol)	ΔG(kJ/mol)	ΔS(J/mol)
0.1	91.95	0.8201	7.07×10^{10}	87.31	66.78	36.79
0.2	164.44	0.9852	3.89×10^{17}	159.80	211.28	-92.25
0.3	175.39	0.9887	1.76×10^{18}	170.75	229.23	-104.82
0.4	182.37	0.9888	3.50×10^{18}	177.73	239.41	-110.53
0.5	189.55	0.9957	7.03×10^{18}	184.91	249.82	-116.31
0.6	171.00	0.9948	4.72×10^{16}	166.36	208.05	-74.72
0.7	116.88	0.9848	1.23×10^{11}	112.24	94.28	32.19
0.8	115.09	0.9861	1.96×10^{10}	110.45	83.97	47.46
0.9	137.88	0.9789	4.46×10^{11}	133.24	121.25	21.49
Average	149.39		1.41×10^{18}	144.75	167.12	-40.08

Table 7
Total mass balance result for the system.

Component	MCHF	GAS	DCMP	CMBPD	ASH	ASFHFG	CFGAS	HPSTM	LPSTM	CWTER1	CWTER
Temperature (°C)	20.0000	20.0000	230.0000	1000.0000	1000.0000	1000.0000	55.0000	597.2173	191.5928	40.0000	47.7808
Pressure (bar)	1.0130	1.0130	1.0130	1.0130	1.0060	1.0060	1.0060	100.0000	5.0000	5.0000	100.0000
Mass Flows (kg/hr)	100.0000	525.0000	99.9999	624.9999	13.3291	611.6708	611.6708	200.0000	200.0000	200.0000	200.0000
WATER	10.0000	-	-	48.8603	-	48.8603	48.8603	200.0000	200.0000	200.0000	200.0000
MCHF	89.8660	-	-	-	-	-	-	-	-	-	-
NITRO-01	-	402.7186	-	402.7186	-	402.7186	402.7186	-	-	-	-
OXYGE-01	-	122.2814	-	Trace	-	Trace	Trace	-	-	-	-
NITRI-01	-	-	-	Trace	-	Trace	Trace	-	-	-	-
NITRO-02	-	-	-	Trace	-	Trace	Trace	-	-	-	-
HYDRO-01	-	-	-	0.0295	-	0.0295	0.0295	-	-	-	-
CARBO-01	-	-	-	0.8953	-	0.8953	0.8953	-	-	-	-
CARBO-02	-	-	-	159.1671	-	159.1671	159.1671	-	-	-	-
CELLU	-	-	45.6162	-	-	-					
HCELL	-	-	15.5095	-	-	-					
LIG-H	-	-	1.8246	-	-	-					
LIG-G	-	-	7.2986	-	-	-					
LIG-S	-	-	16.4218	-	-	-					
POTAS-01	0.0727	-	6.1126	6.1126	6.1126	-					
CALCI-01	0.0139	-	1.1860	1.1860	1.1860	-					
MAGNE-01	0.0160	-	1.4506	1.4506	1.4506	-					
ALUMI-01	0.0176	-	2.7552	2.7552	2.7552	-					
IRON	0.0134	-	1.0948	1.0948	1.0948	-					
SODIU-01	0.0004	-	0.7299	0.7299	0.7299	-					
NITRO-03	-	-	-	Trace	-	Trace	Trace	-	-	-	-

MCHF: millet chaff; DCMP: decomposed product; CMBPD: combustion product; ASFHFG: ash-free hot flue gas; CFGAS: cold flue gas; HPSTM: high pressure steam; LPSTM: low pressure steam; CWTER: cold water; CWTER1: cold water stream-1; Trace: values<10^{-4}

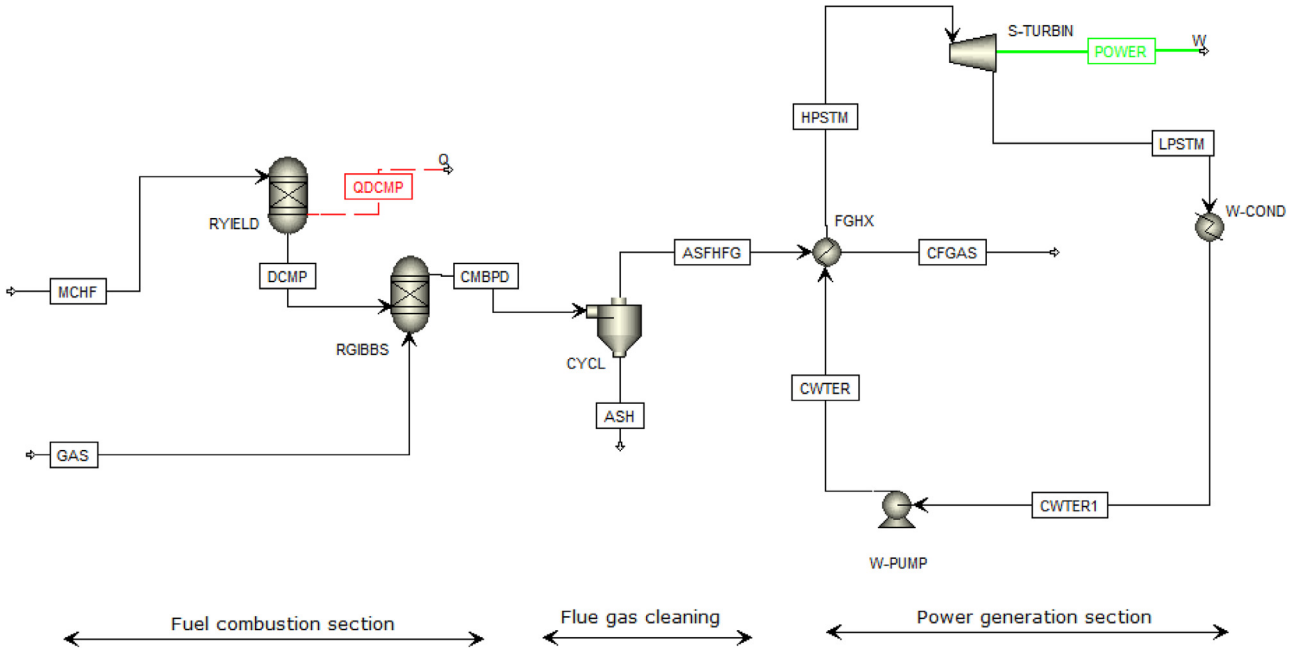

Fig. 11. Process flowsheet of millet chaff combustion coupled with steam turbine for power generation.

heat with ash-free flue gas (ASFHFG), which produced high pressure superheated steam (HPSTM) at 597 ˚C and 10 MPa. The steam is then channelled into S-TURBIN where it expands and converts steam energy to mechanical power that drives an electrical generator. Low pressure steam (LPSTM) (0.5 MPa) from the TURBIN contains some heat energy that can be used as utility within the system. The condensate, CWTER1 from the condenser (W-COND) is returned to the pump for cyclic operation. The overall Aspen process flow diagram is shown in Fig. 11.

3.7. Process analysis

Effect of process parameters such as air/ fuel ratio (AFR: w/w) and combustion chamber temperature on the flue gas composition, combustion efficiency, power generation and electric efficiency were evaluated. The simulation result at combustion chamber temperature of 1000 ˚C (From Fig. 12) indicates that the main components of flue gas include CO, CO_2, H_2, H_2O, O_2 with only NO as the main NOx component. At AFR of 1, as expected, incomplete combustion reaction dominates the process, which can be referred to as pure gasification with flue gas constituting 68% syngas (CO: 39 vol%, H_2: 29 vol%) while CO_2 accounts for only 7 vol%. As the AFR increased, the syngas content of the flue gas reduced significantly and became traceable at AFR of 5.14 (Fig. 12). Under the air deficient region (1≤AFR<5.14), NOx production is very limited and concentration of combustion products (CO_2 and H_2O) in the flue gas increased considerably with the increasing AFR. The combustion products attained maximum value (CO_2:17 vol%, H_2O: 13 vol%) at AFR of 5.14 with corresponding combustion efficiency (CE) of 99.90% computed as according to Eq. (20) (Vallero, 2019). This suggests that stoichiometric combustion of millet chaff in the air atmosphere is attained at AFR of 5.14 (w/w). Combustion studies of Napier grass bagasse reported in the literature shows the stoichiometric AFR of around 4.76 with similar combustion efficiency (Mohammed et al., 2019). Studies by Barmina et al. (2012) also reveal that each biomass material has an individual stoichiometric AFR requirement for complete combustion. This results in specific combustion characteristics due to diverse physicochemical properties of the fuel. Consequently, determination of the stoichiometric AFR of biomass is necessary for assuring the complete combustion of volatiles during the thermochemical conversion.

$$CE = \frac{[CO_2]}{\{[CO_2] + [CO]\}} \tag{20}$$

Where $[CO_2]$ and $[CO]$ is concentration of the CO_2 and CO in the flue gas.

Under the excess air condition (5.14<AFR≤10) (Fig. 12), the O_2 content in the flue gas increased from 0.13 vol% to 9.0 vol%, which translated to 0.62% to 43% excess air while the combustion efficiency remained at 99.9%. The CO_2 and H_2O contents of the flue gas depicted a downward trend in a linear fashion from 17 vol% and 13 vol% respectively at the theoretical air condition to nearly 10 vol% and 7 vol% at 43% excess air condition. This observation could be due to dilution of flue gas by other non-combustion flue gas components emanated from the excess air condition. Consequently, millet chaff combustor can operate efficiently under excess air of up to 43% the stoichiometric air requirement. Generally, combustion reactors are designed to operate on specific amounts of excess air typically in the range of 10-20%. This is to prevent explosion and generation of high temperatures in the system (Vallero, 2019). The NOx generation under the excess air condition increased from 1.6×10^{-7} vol% to 2.3×10^{-2} vol% (at 1000 ˚C combustion chamber temperature), which can be attributed to different combustion parameters (Khan et al., 2009). According to Li and Chyang (2020), NOx emissions are linked to the combined effect of combustion chamber temperature and excess air owing to the improved oxidant and combustion reaction rate. With fuel-nitrogen NOx mechanisms being the dominant mechanism in biomass combustion (Ozgen et al., 2021), the biomass first produces volatile-N and subsequently converted into NHi radicals through gas phase combustion that is further oxidised to NOx in oxygen rich conditions as exhibited in Fig. 12. The result further elucidates that increasing excess air during the combustion of millet chaff generates an increment in the NOx value. A clear approximation of this trend showed that for 10, 20 and 30% excess air, the corresponding NOx value recorded was in 2-fold, 3-fold and 4-folds relative to the NOx value at the theoretical air requirement while there were no significant changes in the NOx value for excess air of 30-40%. This result is in good agreement with NOx values generated during combustion of rice husk, peanut shell, saw dust under the excess air conditions as reported by Li and

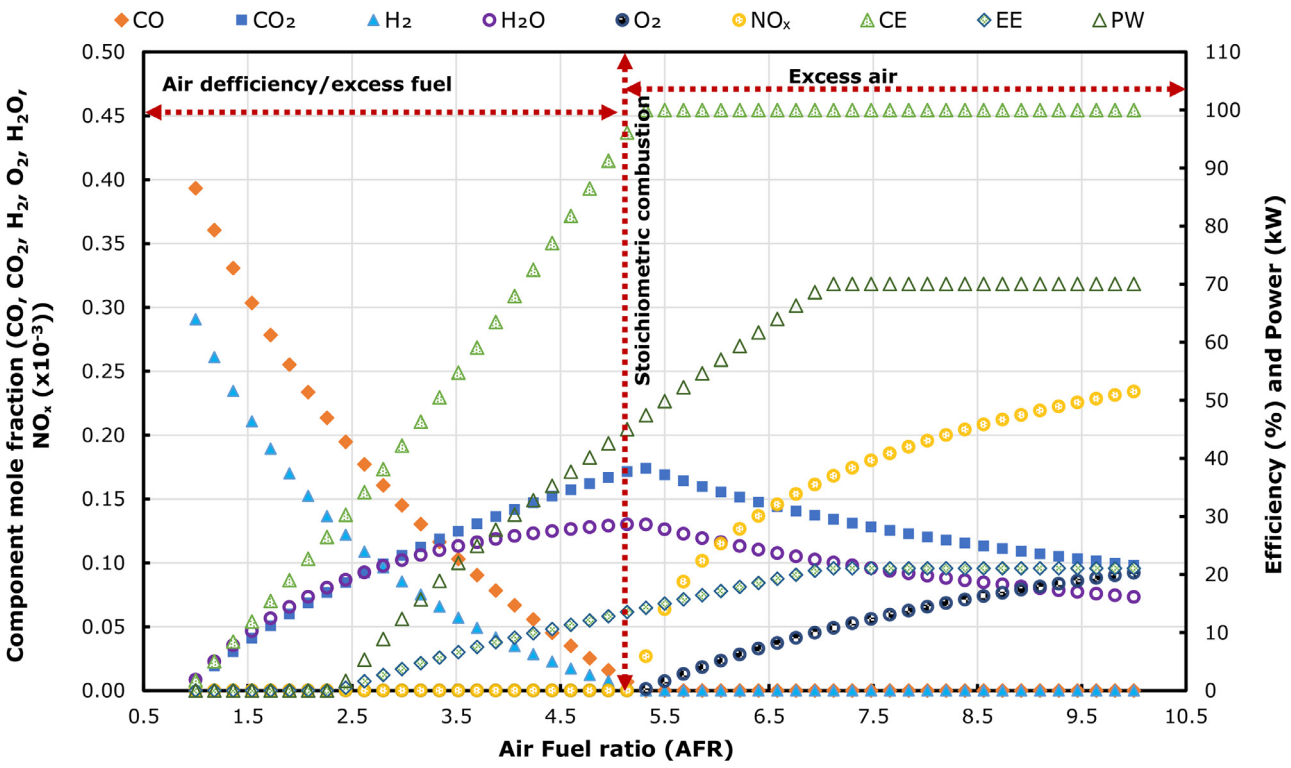

Fig. 12. Effect of Air-fuel ratio on flue gas composition, power generation and process efficiency at combustion chamber temperature of 1000 ˚C (CE: combustion efficiency; EE: electric efficiency; PW: power generation).

Chyang (2020). The authors revealed that when the excess air increases there are corresponding increments in the NOx values for most of the biomass fuels. Combustion of millet chaff under the excess air up to 43% generates NOx level of 282.2 mg/m^3. This value is extremely below the NOx limit value of 650 mg/m^3 (Silva et al., 2021), suggesting the biomass is a good feedstock for power generation. The power generation increased with increasing AFR due to corresponding increase in the flue gas rate (Fig. 12). At AFR of 2.44, 1.66 kW was recorded, which increased to a maximum value of 70 kW at AFR of 7.12, corresponding to excess air of 24%. Similarly, the electric efficiency (EE), which is the ratio of net power output or generated to the thermal input of feedstock computed according to the Eq. (21) increased with increasing AFR. At theoretical AFR, 13.54% EE was recorded, which attained a maximum value of 21.07% under the excess air value of 24%. This result of electric efficiency is similar to the values reported by Godswill (2014). The author recorded 23% electric efficiency for biomass fired power plants with steam turbines. This suggests that millet chaff is a potential feedstock for power generation.

$$EE = \frac{P_{gen}}{\dot{M}_f * LHV_{fuel}} \tag{21}$$

(Godswill, 2014)

Where P_{gen}: Net electricity generated, $\dot{M}_f$: mass flow of fuel and LHV_{fuel}:lower heating value of fuel

The effect of combustion chamber temperature on the flue gas composition at 24% excess air was also investigated. From Fig. 13, the result showed that at 24% excess air, there is no significant changes in the combustion products (CO_2 and H_2O) despite the increasing temperature while also maintaining 99.9% CE. Increase in temperature beyond 1030 ˚C, results in the trace production of CO and H_2 in the flue gas from a nearly zero concentration to 1.94×10^{-6} and 5.94×10^{-7} vol% respectively at 1200˚C. This suggests a probable slow thermal reduction of CO_2 into CO and water-splitting reaction of steam into H_2. Studies have been reported on CO_2 reduction by the reverse water gas shift reaction (Nakano and Bennett, 2014; Wenzel et al., 2017; Zhao et al., 2018). It was stated that this approach could only be sustainable if the energy for the process and H_2 production is supplied from renewable sources as dissociation of CO_2 and H_2O into CO and H_2 requires a large amount of heat for the reaction to be spontaneous (Nakano and Bennett, 2014). With the exothermic nature of the combustion process, the heat requirement to affect the reactions may be satisfied. Therefore, emission of CO_2 associated with biomass firing for power generation via combustion process may possibly serve as another source of hydrocarbon production. The NOx emissions increased exponentially with increasing combustion chamber temperature. This is not surprising as NOx emission is linked to combustion chamber temperature due to the improved combustion reaction rate as earlier stated. This observation provides additional evidence that biomass combustion may not only be associated with NOx formation dominated by the fuel-N mechanism but also thermal NOx mechanism due to oxidation of nitrogen components of air with increasing temperatures (Ozgen et al., 2021). Under the excess air condition, the NOx concentration in the flue gas increased from 1.68×10^{-2} vol% (206.13 mg/m^3) to 5.23×10^{-2} vol% (641.72 mg/m^3) within 200 ˚C raise in the combustion chamber temperature. Studies by Ma et al. (2022) on the release of volatile during biomass combustion in O_2/air atmosphere revealed that NOx production increased with increasing combustion chamber temperature. The authors recorded NOx value in the range of 99.34 mg/m^3 at 700˚C, which increased to 255.21 mg/m^3 when the temperature increased to 1300˚C. Consequently, the values of NOx recorded under the 24% excess air condition are still within the threshold of 650 mg/m^3 NOx emission limit for biomass fired power plant despite the increasing chamber temperature. The power generation increased by 17% per 200˚C raise in the chamber temperature with corresponding increase in the EE value from 21.07% to 24.70% under the excess air condition. This is probably due to the rise in steam temperature from the boiler, which translates to increase in steam quality at the turbine inlet flow (Ganjehkaviri et al., 2015). Therefore, millet chaff combustion under the excess air condition

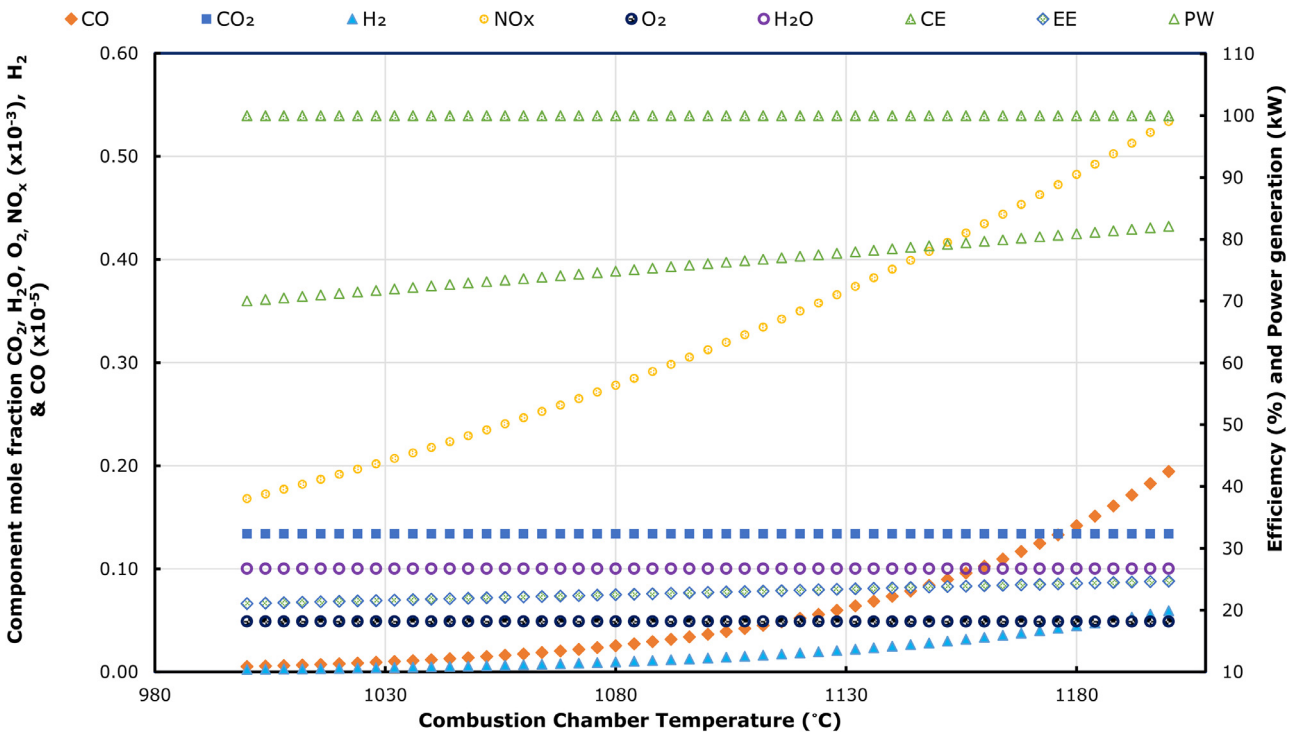

Fig. 13. Effect of combustion chamber temperature on flue gas composition, power generation and process efficiency at 5.68 AFR (20% excess air), CE: combustion efficiency; EE: electric efficiency; PW: power generation.

could improve the thermal efficiency of the power cycle without significant impact on the environment. Consequently, with 1tonne of millet chaff biomass, about 0.7 MWh of electricity could be generated, which translate to additional income. The waste-to-energy strategy if implemented would promote access to clean energy and improve the leaving standards of farmers.

4. Conclusion

Millet chaff constitutes one of the most abundant underutilised agro-residues with zero to little known applications. Information on physicochemical characteristics and energy recovery from millet chaff is currently very limited. This study presents comprehensive physicochemical and combustion characteristics of millet chaff via thermogravimetric analysis and process simulation using Aspen Plus software V11. The proximate analysis result showed 71.25 wt%, 15.35 wt%, 13.40 wt% and 13.15 MJ/kg for volatile matter, fixed-carbon, ash content and higher heating value respectively. The major inorganic mineral elements quantitatively detected in the ash were potassium, aluminium, magnesium, calcium, iron and sodium, suggesting possible slagging and fouling tendencies during combustion. However, these inorganic components are soluble in water and could be leached out easily. The material exhibited low nitrogen and sulphur content from the ultimate analysis. The thermogravimetric analysis revealed an average frequency factor and activation energy of $1.41 \times 10^{18}(s^{-1})$ and 149.39 kJ/mol. The ignition and burnout temperature recorded were in the range of 232-244°C and 430-489°C respectively, which is neither too low nor too high, suggesting a good quality fuel. The average combustion thermodynamic parameters recorded ΔH, ΔG and ΔS were 144.75 kJ/mol, 167.12 kJ/mol and -40.08 J/mol, indicating the characteristics of a good bioenergy feedstock for thermochemical conversion. The combustion process analysis coupled with steam turbine cycle via process simulation revealed an excellent combustion efficiency, good power generation, and good electric efficiency with minimal environmental impacts suitable for clean bioenergy production.

Declaration of Competing Interest

The authors declare that they have no known competing financial interests or personal relationships that could have appeared to influence the work reported in this paper.

Acknowledgments

This work was supported by the TETFund National Research Fund (Project No: TETF/DR&D/CE/NRF/UNI/ATBU/STI/45/Vol.1). Authors also acknowledge the support from Chemical Engineering ATBU PZ/NOTAP Laboratory and the University of Nottingham.

References

BS EN 15290, 2011. Solid biofuels — Determination of major elements — Al, Ca, Fe, Mg, P, K, Si, Na and Ti. British Standards Institution.
BS EN 15442, 2011. Solid Recovered Fuels — *Methods for Sampling*. British Standards Institution.
Açıkalın, K., Gözke, G., 2021. Thermogravimetric pyrolysis of onion skins: determination of kinetic and thermodynamic parameters for devolatilization stages using the combinations of isoconversional and master plot methods. Bioresour. Technol. 342, 125936.
Adeleke, A.A., Odusote, J.K., Ikubanni, P.P., Lasode, O.A., Malathi, M., Paswan, D., 2020. The ignitability, fuel ratio and ash fusion temperatures of torrefied woody biomass. Heliyon 6 (3), e03582 -e03582.
Afgan, N.H., Carvalho, M.G., Jovanovic, M., 2007. Biomass-fired power plant: the sustainability option. Int. J. Sustain. Energy 26 (4), 179–193.
Ahn, H., Kim, D., Lee, Y., 2020. Combustion characteristics of sewage sludge solid fuels produced by drying and hydrothermal carbonization in a fluidized bed. Renew. Energy 147, 957–968.
Ashraf, M., Ramzan, N., Khan, R.U., Durrani, A.K., 2021. Analysis of mixed cattle manure: Kinetics and thermodynamic comparison of pyrolysis and combustion processes. Case Stud. Therm. Eng. 26, 101078.
Ayiania, M., Carbajal-Gamarra, F.M., Garcia-Perez, T., Frear, C., Suliman, W., Garcia-Perez, M., 2019. Production and characterization of H2S and PO43– carbonaceous adsorbents from anaerobic digested fibers. Biomass Bioenergy 120, 339–349.
Barmina, I., Lickrastina, A., Zake, M., Arshanitsa, A., Solodovnik, V., Telysheva, G., 2012. Effect of biomass composition on combustion characteristics and energy quality. International Conference on Renewable Energies and Power Quality.
Barzegar, R., Yozgatligil, A., Olgun, H., Atimtay, A.T., 2020. TGA and kinetic study of different torrefaction conditions of wood biomass under air and oxy-fuel combustion atmospheres. J. Energy Inst. 93 (3), 889–898.

Bermúdez, C.A., Porteiro, J., Varela, L.G., Chapela, S., Patiño, D., 2020. Three-dimensional CFD simulation of a large-scale grate-fired biomass furnace. Fuel Process. Technol. 198, 106219.
Bi, H., Wang, C., Lin, Q., Jiang, X., Jiang, C., Bao, L., 2020. Combustion behavior, kinetics, gas emission characteristics and artificial neural network modeling of coal gangue and biomass via TG-FTIR. Energy 213, 118790.
Boubacar Laougé, Z., Merdun, H., 2020. Kinetic analysis of Pearl Millet (Penissetum glaucum (L.) R. Br.) under pyrolysis and combustion to investigate its bioenergy potential. Fuel 267, 117172.
Chen, L., Wen, C., Wang, W., Liu, T., Liu, E., Liu, H., Li, Z., 2020. Combustion behaviour of biochars thermally pretreated via torrefaction, slow pyrolysis, or hydrothermal carbonisation and co-fired with pulverised coal. Renew. Energy 161, 867–877.
Ciuta, S., Tsiamis, D., Castaldi, M.J., 2018. Chapter six - critical development needs. In: Ciuta, S., Tsiamis, D., Castaldi, M.J. (Eds.), Gasification of Waste Materials. Academic Press, pp. 121–141.
Cuoci, A., Saufi, A.E., Frassoldati, A., Dietrich, D.L., Williams, F.A., Faravelli, T., 2017. Flame extinction and low-temperature combustion of isolated fuel droplets of n-alkanes. Proc. Combust. Inst. 36 (2), 2531–2539.
Fang, S., Yu, Z., Ma, X., Lin, Y., Chen, L., Liao, Y., 2018. Analysis of catalytic pyrolysis of municipal solid waste and paper sludge using TG-FTIR, Py-GC/MS and DAEM (distributed activation energy model). Energy 143, 517–532.
Fantozzi, F., Bartocci, P, 2017. 4 - Biomass feedstock for IGCC systems. In: Wang, T., Stiegel, G. (Eds.), Integrated Gasification Combined Cycle (IGCC) Technologies. Woodhead Publishing, pp. 145–180.
Fong, M.J.B., Loy, A.C.M., Chin, B.L.F., Lam, M.K., Yusup, S., Jawad, Z.A., 2019. Catalytic pyrolysis of Chlorella vulgaris: kinetic and thermodynamic analysis. Bioresour. Technol. 289, 121689.
Ganjehkaviri, A., Mohd Jaafar, M.N., Hosseini, S.E., 2015. Optimization and the effect of steam turbine outlet quality on the output power of a combined cycle power plant. Energy Convers. Manage. 89, 231–243.
Godswill, U.M., 2014. Process simulations of small scale biomass power plant (Dissertation). School of Engineering. Vol. MSc University of Borås.
Guo, F., He, Y., Hassanpour, A., Gardy, J., Zhong, Z., 2020. Thermogravimetric analysis on the co-combustion of biomass pellets with lignite and bituminous coal. Energy 197, 117147.
Islam, M.A., Auta, M., Kabir, G., Hameed, B.H., 2016. A thermogravimetric analysis of the combustion kinetics of karanja (Pongamia pinnata) fruit hulls char. Bioresour. Technol. 200, 335–341.
Jianfei, Y., Zixing, F., Liangmeng, N., Qi, G., Zhijia, L., 2020. Combustion characteristics of bamboo lignin from kraft pulping: influence of washing process. Renew. Energy 162, 525–534.
Karuppasamy Vikraman, V., Praveen Kumar, D., Boopathi, G., Subramanian, P., 2021. Kinetic and thermodynamic study of finger millet straw pyrolysis through thermogravimetric analysis. Bioresour. Technol. 342, 125992.
Khan, A.A., de Jong, W., Jansens, P.J., Spliethoff, H., 2009. Biomass combustion in fluidized bed boilers: potential problems and remedies. Fuel Process. Technol. 90 (1), 21–50.
Kim, Y.S., Kim, Y.S., Kim, S.H., 2010. Investigation of thermodynamic parameters in the thermal decomposition of plastic waste−waste lube oil compounds. Environ. Sci. Technol. 44 (13), 5313–5317.
Li, P.-W., Chyang, C.-S., 2020. A comprehensive study on NOx emission and fuel nitrogen conversion of solid biomass in bubbling fluidized beds under staged combustion. J. Energy Inst. 93 (1), 324–334.
Liu, J., Zhong, F., Niu, W., Su, J., Gao, Z., Zhang, K., 2019. Effects of heating rate and gas atmosphere on the pyrolysis and combustion characteristics of different crop residues and the kinetics analysis. Energy 175, 320–332.
Lu, J.-J., Chen, W.-H., 2015. Investigation on the ignition and burnout temperatures of bamboo and sugarcane bagasse by thermogravimetric analysis. Appl. Energy 160, 49–57.
Ma, R., Fan, W., Wang, X., Chen, J., Wu, X., 2022. Conversion of volatile nitrogen and char nitrogen to NO in oxy-biomass combustion. J. Energy Inst. 100, 120–128.
Maia, A.A.D., Enriquez, Y.A.M., de Morais, L.C., 2020. Experimental investigation of the delignification process influence on thermochemical and kinetic properties of biomass. J. Therm. Anal. Calorim. 1–11.
Miura, K., Maki, T., 1998. A simple method for estimating f(E) and k0(E) in the distributed activation energy model. Energy Fuels 12 (5), 864–869.
Mlonka-Mędrala, A., Magdziarz, A., Gajek, M., Nowińska, K., Nowak, W., 2020. Alkali metals association in biomass and their impact on ash melting behaviour. Fuel 261, 116421.
Mohammed, I., Abakr, Y., Kazi, F., Yusup, S., Alshareef, I., Chin, S., 2015. Comprehensive characterization of napier grass as a feedstock for thermochemical conversion. Energies 8 (5), 3403–3417.
Mohammed, I.Y., Abakr, Y.A., Kazi, F.K., Yusuf, S., 2017a. Effects of pretreatments of Napier grass with deionized water, sulfuric acid and sodium hydroxide on pyrolysis oil characteristics. Waste Biomass Valoriz. 8 (3), 755–773.
Mohammed, I.Y., Abakr, Y.A., Mokaya, R., 2019. Integrated biomass thermochemical conversion for clean energy production: process design and economic analysis. J. Environ. Chem. Eng. 7 (3), 103093.
Mohammed, I.Y., Abakr, Y.A., Mokaya, R., 2018a. Valorisation of adzuki bean waste to biofuel precursors via pyrolysis: kinetics, product distribution and characterisation. Biomass Convers. Biorefinery 8 (3), 699–710.
Mohammed, I.Y., Abakr, Y.A., Xing Hui, J.N., Alaba, P.A., Morris, K.I., Ibrahim, M.D., 2017b. Recovery of clean energy precursors from Bambara groundnut waste via pyrolysis: kinetics, products distribution and optimisation using response surface methodology. J. Clean. Prod. 164, 1430–1445.
Mohammed, I.Y., Abakr, Y.A., Yusup, S., Kazi, F.K., 2017c. Valorization of Napier grass via intermediate pyrolysis: optimization using response surface methodology and pyrolysis products characterization. J. Clean. Prod. 142, 1848–1866.
Mohammed, I.Y., Abba, Z., Matias-Peralta, H.M., Abakr, Y.A., Fuzi, S.F.Z.M., 2018b. Thermogravimetric study and evolved gas analysis of new microalga using TGA-GC-MS. Biomass Convers. Biorefinery 8 (3), 669–678.
Nakano, J., Bennett, J., 2014. CO2 and H2O gas conversion into CO and H2 using highly exothermic reactions induced by mixed industrial slags. Int. J. Hydrogen Energy 39 (10), 4954–4958.
Navarro, M.V., López, J.M., Veses, A., Callén, M.S., García, T., 2018. Kinetic study for the co-pyrolysis of lignocellulosic biomass and plastics using the distributed activation energy model. Energy 165, 731–742.
Nazli, R.I., 2020. Evaluation of different sweet sorghum cultivars for bioethanol yield potential and bagasse combustion characteristics in a semiarid Mediterranean environment. Biomass Bioenergy 139, 105624.
Nematpour, A., Eshghizadeh, H.R., Zahedi, M., Gheysari, M., 2020. Interactive effects of sowing date and nitrogen fertilizer on water and nitrogen use efficiency in millet cultivars under drought stress. J. Plant Nutr. 43 (1), 122–137.
Ortiz, L.R., Torres, E., Zalazar, D., Zhang, H., Rodriguez, R., Mazza, G., 2020. Influence of pyrolysis temperature and bio-waste composition on biochar characteristics. Renew. Energy 155, 837–847.
Ozgen, S., Cernuschi, S., Caserini, S., 2021. An overview of nitrogen oxides emissions from biomass combustion for domestic heat production. Renew. Sustain. Energy Rev. 135, 110113.
Parthasarathy, P., Fernandez, A., Al-Ansari, T., Mackey, H.R., Rodriguez, R., McKay, G., 2021. Thermal degradation characteristics and gasification kinetics of camel manure using thermogravimetric analysis. J. Environ. Manage. 287, 112345.
Reza, M.S., Islam, S.N., Afroze, S., Bakar, M.S.A., Taweekun, J., Azad, A.K., 2020. Data on FTIR, TGA – DTG, DSC of invasive pennisetum purpureum grass. Data Brief 30, 105536.
Ryden, P., Efthymiou, M.-N., Tindyebwa, T.A., Elliston, A., Wilson, D.R., Waldron, K.W., Malakar, P.K., 2017. Bioethanol production from spent mushroom compost derived from chaff of millet and sorghum. Biotechnol. Biofuels 10 (1), 1–11.
Sajjad Ahmad, M., Liu, H., Alhumade, H., Hussain Tahir, M., Çakman, G., Yıldız, A., Ceylan, S., Elkamel, A., Shen, B., 2020. A modified DAEM: to study the bioenergy potential of invasive Staghorn Sumac through pyrolysis, ANN, TGA, kinetic modeling, FTIR and GC–MS analysis. Energy Convers. Manage. 221, 113173.
Silva, J.P., Teixeira, S., Grilo, É., Peters, B., Teixeira, J.C., 2021. Analysis and monitoring of the combustion performance in a biomass power plant. Clean. Eng. Technol. 5, 100334.
Smith, J.D., Sreedharan, V., Landon, M., Smith, Z.P., 2020. Advanced design optimization of combustion equipment for biomass combustion. Renew. Energy 145, 1597–1607.
Szűcs, T., Szentannai, P., Szilágyi, I.M., Bakos, L.P., 2020. Comparing different reaction models for combustion kinetics of solid recovered fuel. J. Therm. Anal. Calorim. 139 (1), 555–565.
Thoharudin, Hsiau, S.-S., Chen, Y.-S., Yang, S., 2022. Numerical simulation of fluidized bed pyrolysis under a simplified comprehensive multistep kinetic mechanism: Effects of particle size and fluidization velocity. Energy Convers. Manage. 254, 115259.
Vallero, D.A, 2019. Chapter 9 - thermal reactions. In: Vallero, D.A. (Ed.), Air Pollution Calculations. Elsevier, pp. 207–218.
Várhegyi, G., Szabó, P., Antal, M.J., 2002. Kinetics of charcoal devolatilization. Energy Fuels 16 (3), 724–731.
Vyazovkin, S., Burnham, A.K., Criado, J.M., Pérez-Maqueda, L.A., Popescu, C., Sbirrazzuoli, N., 2011. ICTAC Kinetics Committee recommendations for performing kinetic computations on thermal analysis data. Thermochim. Acta 520 (1), 1–19.
Wang, Y., Tan, H., Wang, X., Du, W., Mikulčić, H., Duić, N., 2017. Study on extracting available salt from straw/woody biomass ashes and predicting its slagging/fouling tendency. J. Clean. Prod. 155, 164–171.
Wenzel, M., Aditya Dharanipragada, N.V.R., Galvita, V.V., Poelman, H., Marin, G.B., Rihko-Struckmann, L., Sundmacher, K., 2017. CO production from CO2 via reverse water–gas shift reaction performed in a chemical looping mode: Kinetics on modified iron oxide. J. CO2 Utiliz. 17, 60–68.
Xu, J., Liu, X., Wu, J., Zhang, Y. An effective method to remove organic sulfur in coal: Effects on the physicochemical properties and combustion kinetics. *Environ. Prog. Sustain. Energy*, e13779.
Xu, Y., Chen, B., 2013. Investigation of thermodynamic parameters in the pyrolysis conversion of biomass and manure to biochars using thermogravimetric analysis. Bioresour. Technol. 146, 485–493.
Yan, J., Liu, M., Feng, Z., Bai, Z., Shui, H., Li, Z., Lei, Z., Wang, Z., Ren, S., Kang, S., 2020. Study on the pyrolysis kinetics of low-medium rank coals with distributed activation energy model. Fuel 261, 116359.
Zhao, K., Bkour, Q., Hou, X., Kang, S.W., Park, J.C., Norton, M.G., Yang, J.-I., Ha, S., 2018. Reverse water gas shift reaction over CuFe/Al2O3 catalyst in solid oxide electrolysis cell. Chem. Eng. J. 336, 20–27.
Zou, H., Li, W., Liu, J., Buyukada, M., Evrendilek, F., 2020. Catalytic combustion performances, kinetics, reaction mechanisms and gas emissions of Lentinus edodes. Bioresour. Technol. 300, 122630.